Revision 1

Crystal-chemistry of sulfates from the Apuan Alps (Tuscany, Italy). VI. Tl-bearing alum-(K) and voltaite from the Fornovolasco mining complex

CRISTIAN BIAGIONI[1*], DANIELA MAURO[1], MARCO PASERO[1], ELENA BONACCORSI[1], GIOVANNI ORAZIO LEPORE[2], FEDERICA ZACCARINI[3] and HENRIK SKOGBY[4]

[1] *Dipartimento di Scienze della Terra, Università di Pisa, Via S. Maria 53, I-56126 Pisa, Italy*

[2] *CNR-IOM-OGG c/o ESRF, 71 Avenue des Martyrs CS 40220 F-38043 Grenoble Cedex 9, Grenoble, France*

[3] *Department of Applied Geological Sciences and Geophysics, University of Leoben, Peter Tunner Str. 5, A-8700 Leoben, Austria*

[4] *Department of Geosciences, Swedish Museum of Natural History, Box 50007, SE-10405 Stockholm, Sweden*

**e-mail address: cristian.biagioni@unipi.it*

This is a preprint, the final version is subject to change, of the American Mineralogist (MSA)
Cite as Authors (Year) Title. American Mineralogist, in press.
DOI: https://doi.org/10.2138/am-2020-7320

ABSTRACT

Thallium-bearing samples of alum-(K) and voltaite from the Fornovolasco mining complex (Apuan Alps, Tuscany, Italy) have been characterized through X-ray diffraction, chemical analyses, micro-Raman, infrared (FTIR), Mössbauer, and X-ray Absorption Spectroscopy (XAS). Alum-(K) occurs as anhedral colorless grains or rarely as octahedral crystals, up to 0.5 mm. Electron-microprobe analysis points to the chemical formula $(K_{0.74}Tl_{0.10})_{\Sigma 0.84}(Al_{0.84}Fe_{0.14})_{\Sigma 0.98}S_{2.03}O_8 \cdot 12H_2O$. The occurrence of minor NH_4^+ was detected through FTIR spectroscopy. Its unit-cell parameter is a = 12.2030(2) Å, V = 1817.19(9) Å^3, space group $Pa\bar{3}$. Its crystal structure has been refined down to R_1 = 0.0351 for 648 reflections with $F_o > 4\sigma(F_o)$ and 61 refined parameters. The crystal structure refinement agrees with the partial substitution of K by 12 mol% Tl. This substitution is confirmed by XAS data, showing the presence of Tl^+ having a first coordination shell mainly formed by 6 O atoms at 2.84(2) Å. Voltaite occurs as dark green cubic crystals, up to 1 mm in size. Voltaite is chemically zoned, with distinct domains having chemical formula $(K_{1.94}Tl_{0.28})_{\Sigma 2.22}(Fe^{2+}_{3.57}Mg_{0.94}Mn_{0.55})_{\Sigma 5.06}Fe^{3+}_{3.06}Al_{0.98}S_{11.92}O_{48} \cdot 18H_2O$ and $(K_{2.04}Tl_{0.32})_{\Sigma 2.36}(Fe^{2+}_{3.83}Mg_{0.91}Mn_{0.29})_{\Sigma 5.03}Fe^{3+}_{3.05}Al_{0.97}S_{11.92}O_{48} \cdot 18H_2O$, respectively. Infrared spectroscopy confirmed the occurrence of minor NH_4^+ also in voltaite. Its unit-cell parameter is a = 27.2635 Å, V = 20265(4) Å^3, space group $Fd\bar{3}c$. The crystal structure was refined down to R_1 = 0.0434 for 817 reflections with $F_o > 4\sigma(F_o)$ and 87 refined parameters. The partial replacement of K by Tl is confirmed by the structural refinement. XAS spectroscopy showed that Tl^+ is bonded to six O atoms, at 2.89(2) Å. The multi-technique characterization of thallium-bearing alum-(K) and voltaite improves our understanding of the role of K-bearing sulfates in immobilizing Tl in acid mine drainage systems, temporarily avoiding its dispersion in the environment.

Key-words: alum-(K), voltaite, thallium, XAS, crystal structure, Fornovolasco, Apuan Alps, Tuscany, Italy.

Introduction

Thallium (Z = 81) is a toxic heavy element, classified as one of the thirteen priority metal pollutants (Keith and Telliard 1979) and having an average concentration in the upper continental crust of 0.75 μg/g (Wedepohl 1995). Thallium occurs in two different oxidation states, i.e., Tl^{+} and Tl^{3+}. Monovalent Tl has both a lithophile and chalcophile geochemical behavior, being enriched in K-bearing minerals as well as in several chalcogenides. In particular, the ionic radius of Tl^{+} is close to that of K^{+} and Rb^{+} (e.g., Shannon, 1976). Indeed, the only three secondary Tl^{+}-minerals known up to now as products of sulfide weathering, i.e. dorallcharite, $TlFe^{3+}_3(SO_4)_2(OH)_6$ (Balić-Žunić et al. 1994), lanmuchangite, $TlAl(SO_4)_2 \cdot 12H_2O$ (Chen and Wang 2001), and thalliumpharmacosiderite, $TlFe_4(AsO_4)_3(OH)_4 \cdot 4H_2O$ (Rumsey et al. 2014), are the counterparts of the K-minerals jarosite, alum-(K), and pharmacosiderite, respectively. Götz et al. (1968) described "monsmedite" as a new K-Tl^{3+} sulfate, with approximate chemical formula $Tl_2O_3 \cdot K_2O \cdot 8SO_3 \cdot 15H_2O$. This species was later discredited by the then IMA-CNMMN (Grice and Ferraris 2003) and the reinvestigation of several samples and co-type material by some authors (e.g., Johan et al. 2009; Kovács-Pálffy et al. 2011) showed that "monsmedite" is simply Tl-bearing voltaite.

The identification of the thallium-rich nature of the pyrite ore deposits of the southern Apuan Alps (northern Tuscany, Italy), with up to more than 4000 μg/g Tl (Biagioni et al. 2013; George et al. 2018) gave rise to a series of mineralogical and geochemical studies which led to the description of the dispersion of thallium in the environment (D'Orazio et al. 2017; Biagioni et al. 2017; Perotti et al. 2018; Ghezzi et al. 2019). Sulfate assemblages play a major role in the control of the release of heavy metals in the environment and their mineralogical characterization is being currently undertaken. Our attention is mainly focused on the assemblages found in the Fornovolasco mining complex, where the highest Tl contents in pyrite ores have been reported (e.g., D'Orazio et al. 2017). Since the first description of volaschioite (Biagioni et al. 2011), more than fifteen different

sulfate species have been identified in this locality. Among them, the two K-sulfates alum-(K) and voltaite are particularly interesting, owing to their significant Tl content.

The aim of this paper is the full characterization of Tl-bearing alum-(K) and voltaite from Fornovolasco (Apuan Alps, Tuscany, Italy), providing data for assessing the role played by K-sulfates in the transient sequestration of thallium in the acid mine drainage systems. Therefore, these minerals have been characterized through single-crystal X-ray diffraction, electron microprobe analysis, and some spectroscopic techniques, i.e., micro-Raman, infrared, Mössbauer and X-ray Absorption Spectroscopy (XAS).

Experimental

The studied specimens (Fig. 1) were collected in the 740 m level of the pyrite – iron oxide mine of Fornovolasco (Apuan Alps, Tuscany, Italy). Alum-(K) occurs as crude colorless octahedral crystals, up to 0.5 mm in size, associated with römerite, copiapite, and minor voltaite. Voltaite occurs as cubic crystals, with minor octahedral and rombic dodecahedral faces, dark green in color, up to 1 mm, usually associated with halotrichite and römerite.

Quantitative chemical data were collected on these samples through a Superprobe JEOL JXA 8200 electron microprobe at the "Eugen F. Stumpfl" laboratory (Leoben University, Austria). The following analytical conditions were used: WDS mode, accelerating voltage 10 kV (15 kV for thallium analysis), beam current 10 nA. Beam size was set to 20 μm in order to minimize sample damage. Standards were (element, emission line): magnetite (Fe*K*α), TlBr (Tl*M*α), sanidine (K*K*α), albite (Al*K*α), olivine (Mg*K*α), rhodonite (Mn*K*α), and baryte (S*K*α). The ZAF routine was applied for the correction of the recorded raw data. Counting times were 15 s for peak and 5 s for left and right backgrounds. Several difficulties occurred during the preparation and the analysis of sulfate samples, mainly related to their instability under the electron beam and the high vacuum, and for the burst of the fluid inclusions entrapped in the analyzed grains, able to destroy the carbon coating and the polished surface. These inconveniences were particularly critical during the analysis of alum-

(K). Indeed, the electron beam created some pits, several μm across, on the sample, owing to the strong dehydration and the burst of fluid inclusions. Consequently, only one spot analysis, normalized to 100 wt%, was obtained on alum-(K). Back-scattered electron (BSE) images of voltaite showed the occurrence of a strong chemical zonation (see below), studied through X-ray maps whose collection was carried out on the basis of the same analytical conditions used for electron microprobe analyses. Chemical data are given in Table 1.

The ^{57}Fe Mössbauer spectrum of voltaite was collected at room temperature in transmission mode using a ^{57}Co (in Rh matrix) point source with a nominal activity of 0.40 GBq at the Swedish Museum of Natural History, Stockholm, Sweden. Fifteen crystals were mounted on a sticky tape and were positioned closely in front of the point-source. The Mössbauer spectrum was acquired over the velocity range ± 4 mm/s and was calibrated against α-Fe foil. The spectrum was fitted using the program MossA (Prescher et al. 2012).

Micro-Raman spectra of alum-(K) and voltaite were collected on unpolished samples in nearly backscattered geometry using a Jobin-Yvon Horiba XploRA Plus apparatus, equipped with a motorized *x*-*y* stage and an Olympus BX41 microscope with a 10× objective lens. The Raman spectra were excited using a 532 nm line of a solid-state laser attenuated to 10% (2.5 mW) in order to minimize sample damage. The minimum lateral and depth resolution was set to a few μm. The system was calibrated using the 520.6 cm^{-1} Raman band of silicon before each experimental session. Spectrum was collected through multiple acquisitions with single counting times of 120 and 60 s for alum-(K) and voltaite, respectively. Backscattered radiation was analyzed with a 1200 gr/mm grating monochromator. Peak deconvolution was performed using Fityk (Wojdyr 2010).

Unpolarized FTIR absorption spectra of alum-(K) and voltaite were measured on gently powdered sample material mixed with KCl and pressed to a pellet. A Bruker Vertex spectrometer equipped with a Globar source, a KBr beam-splitter, an MCT detector, and a Hyperion 2000 microscope was used to acquire spectra in the wavenumber range 6000–600 cm^{-1} with a resolution of 4 cm^{-1}.

X-ray Absorption Spectroscopy (XAS) measurements at the TlL_3 edge (12658 eV) were performed at the LISA beamline BM 08 (d'Acapito et al. 2019) at the European Synchrotron Radiation Facility (ESRF), Grenoble, France. Measurements on alum-(K) were collected in fluorescence mode by means of a 12-elements solid state (high purity germanium; Puri et al. 2019). A fixed exit sagittally focusing monochromator (d'Acapito et al. 2014) with a pair of Si (311) crystals was used; Pd coated mirrors were used for harmonics rejection ($E_{cutoff} \approx 18$ keV). A few grains of alum-(K) were powdered, mixed with cellulose and pressed in a pellet using an amount of material such as to keep the maximum total absorption (μ) around 1.5. Voltaite was measured with the new BM08 setup (d'Acapito et al. 2019), using a pair of Si (111) flat crystals and Si coated focusing mirrors ($E_{cutoff} \approx 16$ keV); the beam size on the sample was $\approx 200 \times 200$ μm^2. Measurements were taken on a grain of voltaite in fluorescence mode using a Si photodiode detector. Pellets of Tl_2O_3 and Tl_2SO_4 were also measured as model compounds in transmission mode. A reference Se foil (*K*-edge = 12657.8 eV) was also measured at the same time in order to accurately calibrate the energy. The software ATHENA (Ravel and Newville 2005) was used to average multiple spectra. Standard procedures (Lee et al. 1981) were followed to extract the structural EXAFS (Extended X-ray Absorption Fine Structure) signal (k•χ(k)): pre-edge background removal, spline modelling of bare atomic background, edge step normalization using a far above the edge region, and energy calibration. Model atomic clusters centred on the absorber atom were obtained by ATOMS (Ravel 2001) using the crystallographic structure reported in this paper for alum-(K) and voltaite; theoretical amplitude and phase functions were generated using the FEFF8 code (Ankudinov et al. 1998). EXAFS spectra were fitted through the ARTEMIS software (Ravel and Newville 2005) in the Fourier-Transform (FT) space.

Intensity data of alum-(K) and voltaite were collected using a Bruker Smart Breeze single-crystal diffractometer operating at 50 kV and 30 mA and equipped with an air-cooled CCD detector. Graphite-monochromatized Mo*K*α radiation was used. The detector-to-crystal working distance was set to 50 mm. Intensity data were integrated and corrected for Lorentz, polarization,

background effects, and absorption using the package of software APEX 2 (Bruker AXS Inc. 2004). The crystal structures of both minerals were refined using SHELXL-2018 (Sheldrick 2015), starting from the atomic coordinates given by Ballirano (2015) and by Mereiter (1972) for alum-(K) and voltaite, respectively. Taking into account the results of chemical analyses (see below), the following neutral scattering curves, taken from the International Tables for Crystallography (Wilson 1992), were used: for alum-(K), K vs. Tl at the K site, Al vs. Fe at the Al site, S at the S site, and H at the H sites; for voltaite, K vs. Tl at the K site, Fe vs. Mg at the *M*(1) and *M*(2) sites, Al at the Al site, and H at the H sites, respectively. Fully ionized scattering curves were used for O atoms at the O sites in both crystal structure refinements. In the structural refinement of both minerals, a soft restraint on the O–H distance was applied [0.95(2) Å], in order to avoid too short O–H distances. In voltaite, the H atoms belonging to the disordered H_2O groups were not located. After several cycles of anisotropic refinement (with the exception of H atoms, which were refined isotropically), the crystal structure refinements of alum-(K) and voltaite converged to R_1 = 0.0351 (for 648 unique reflections with $F_o > 4\sigma(F_o)$ and 61 refined parameters) and 0.0434 (for 817 unique reflections with $F_o > 4\sigma(F_o)$ and 87 refined parameters), respectively. Details of data collections and crystal structure refinements are given in Table 2. Fractional atomic coordinates, site occupancies, and displacement parameters are reported in Table 3, whereas Table 4 shows selected bond distances for alum-(K) and voltaite. Weighted bond-valence sums (BVS, in valence unit, v.u.), calculated on the basis of the bond parameters given by Brese and O'Keeffe (1991), are given in Table 5.

Results and discussions

Alum-(K): crystal structure, sulfate disorder, and thallium speciation

Alum-(K), $KAl(SO_4)_2 \cdot 12H_2O$, belongs to the alum group, a series of cubic minerals and synthetic compounds characterized by the general formula $X^+Y^{3+}(T^{6+}O_4)_2 \cdot 12H_2O$, where X = Na, K, Rb, Cs, Tl, NH_4, NH_3CH_3, NH_3OH, etc., Y = Al, Cr, Fe, Ga, In, Ru, etc., and T = S or Se (e.g., Nyburg et al. 2000; Ballirano, 2015). In addition to alum-(K), other natural members of the alum

group are alum-(Na) (X = Na, Y = Al), lanmuchangite (X = Tl, Y = Al), tschermigite (X = NH_4, Y = Al), and probably lonecreekite (X = NH_4, Y = Fe). The crystal structure of alum-(K) was first solved by Cork (1927) and later reinvestigated by Beevers and Lipson (1934). In agreement with Lipson (1935), alums are divided into three types, i.e., α-, β-, and γ-type, depending on the orientation of the SO_4 group. This polymorphism seems to be related to the occurrence of monovalent cations with medium (α), small (β), and large (γ) ionic radii. Larson and Cromer (1967) refined the crystal structure of synthetic α-alums (X = K, Rb, and NH_4) and pointed out the occurrence of SO_4 disorder.

The chemical formula of the studied sample of alum-(K), on the basis of 8 O atoms per formula unit (apfu) and assuming the occurrence of 12 H_2O groups, is $(K_{0.74}Tl_{0.10})_{\Sigma 0.84}(Al_{0.84}Fe_{0.14})_{\Sigma 0.98}S_{2.03}O_8 \cdot 12H_2O$. The significant deficit of (K+Tl) can be partly related to the low quality of chemical analysis and K migration under the electron beam (e.g., Craw 1981; van der Pluijm et al. 1988), but it could also mask the presence of an undetected light constituent, such as NH_4. This Tl-bearing sample has a unit-cell parameter (~12.20 Å) intermediate between those of pure synthetic $KAl(SO_4)_2 \cdot 12H_2O$ (hereafter KAl-alum), 12.1640(5) Å, and pure synthetic $TlAl(SO_4)_2 \cdot 12H_2O$ (hereafter TlAl-alum), 12.2305(5) Å. It is worth noting that, if one assumes a linear increase of the unit-cell parameter from KAl-alum to TlAl-alum, the measured *a* value should correspond to ca. 0.40 Tl apfu, neglecting minor Fe^{3+}-to-Al^{3+} substitution. Chemical data, as well as crystal structure refinement (see below), do not support such a high Tl content and it is likely that the substitution of Al^{3+} by Fe^{3+} could contribute to the increase of the unit-cell parameter. However, another component, characterized by a large ionic radius and low *Z* number, should be likely present. As discussed below, this additional component is represented by $(NH_4)^+$, whose ionic radius is similar to that of Tl^+ (compare isotypic compounds TlCl and NH_4Cl – Roberts et al. 2006). Therefore, the increase in the unit-cell parameter is not related to the $K^+ \rightarrow Tl^+$ substitution only, but also to the replacement of K^+ by NH_4^+ and Al^{3+} by Fe^{3+}.

199 The crystal structure of the studied sample agrees with previous determinations (e.g.,
200 Ballirano, 2015): alum-(K) is formed by isolated $Al(H_2O)_6$ octahedra, $K(H_2O)_6$ polyhedra, and SO_4
201 groups (Fig. 2). Hydrogen bonds play an important role in stabilizing the crystal structure.
202 Two SO_4 configurations have been observed, in agreement with previous studies. However,
203 whereas the *k* disorder parameter [i.e., the site occupancy factor of O(3) and O(4) sites] is ~ 0.7 in
204 KAl-alum, a higher value, close to ~ 0.8, occurs in Tl-bearing alum-(K). This is in keeping with the
205 larger ionic radius of Tl^+ (as well as NH_4^+) with respect to K^+ (1.50 vs 1.38 Å in six-fold
206 coordination for Tl^+ and K^+, respectively, according to Shannon 1976). Indeed, the larger the ionic
207 radius of the M^+ cation, the higher the *k* value, e.g., 0.697 and 0.843 in KAl and TlAl synthetic
208 alums (Nyburg et al. 2000). The most probable SO_4 configuration (77%) has average bond distance
209 1.463 Å, with distances ranging from 1.442(5) to 1.470(2) Å; the less probable configuration (23%)
210 has a shorter average bond distance, i.e., 1.459 Å, with distances in the range 1.429(16) – 1.469(8)
211 Å. These values can be compared with the results of Nyburg et al. (2000) and Ballirano (2015), i.e.,
212 1.468 and 1.466 Å for the more frequent configuration, and 1.450 Å for the less frequent one.
213 Moreover, these values can be compared with the grand <S–O> distance of 1.473 Å reported by
214 Hawthorne et al. (2000). The shortening of S–O distances in alum-(K) has been attributed to
215 libration effects (Nyburg et al. 2000). The corresponding weighted bond-valence sum is 6.21
216 valence unit (v.u.); actually it is 6.19 and 6.25 v.u. for the more and less frequent configurations,
217 respectively. The occurrence of two distinct configurations of SO_4 group results in the appearance,
218 in the Raman spectrum of alum-(K) (Fig. 3a), of two close bands having different intensities; such a
219 difference is directly related to differences in the site occupancy at the O(3)/O(3)A and O(4)/O(4)A
220 sites. The intensity ratio between the two bands related to the ν_1 stretching mode of SO_4 groups
221 (Fig. 3a) is 75/25, very close to the 77/23 ratio obtained through single-crystal structure refinement.
222 The Raman spectrum of alum-(K) shows other spectral features related to vibrational modes of SO_4
223 groups (Fig. 3a), in agreement with Frost and Kloprogge (2001).

The Al–O bond distance, 1.8946(14) Å, is larger than those observed by Nyburg et al. (2000) and Ballirano (2015), i.e., 1.875(1) and 1.868(2) Å. This is likely the result of the replacement of Al^{3+} by Fe^{3+}, giving the site occupancy ($Al_{0.88}Fe_{0.12}$), in good agreement with chemical data. The occurrence of Fe^{3+} in alum-(K) suggests the possible existence of the end-member composition $KFe^{3+}(SO_4)_2 \cdot 12H_2O$, the K-analogue of lonecreekite (Martini, 1983). On the basis of these s.o.f., the calculated BVS is 3.24 v.u.

The K site hosts K^+, partially replaced by Tl^+ and $(NH_4)^+$; the refined site occupancy is ($K_{0.88}Tl_{0.12}$). The occurrence of NH_4 is confirmed by FTIR spectroscopy showing a band occurring at 1443 cm^{-1} (Fig. 3b), in agreement with the value reported in tschermigite (e.g., Zhitova et al. 2019). These monovalent cations are coordinated by six H_2O groups in an almost flat "crown" coordination, with bond distance of 2.9974(19) Å. This distance is longer than that observed in KAl-alum by Nyburg et al. (2000) and Ballirano (2015), i.e., 2.954(1) and 2.947(2) Å, respectively, as a result of the replacement of K^+ by the larger Tl^+ and NH_4^+. Two additional bond distances are associated with the occurrence of the less frequent SO_4 configuration, i.e., 2.618(16) Å, to be compared with the value reported by Nyburg et al. (2000) and Ballirano (2015), i.e., 2.636(5) and 2.6348(18) Å. Larson and Cromer (1967) suggested that the K site may be split into two sub-positions, in order to avoid the K–O(3)A bonds. However, as pointed out by Ballirano (2015), this model would result in a too low BVS [0.66 v.u. according to Ballirano 2015; 0.58 v.u. in the present refinement of Tl-bearing alum-(K)]. Consequently, this author proposed that a seven-fold coordination or, alternatively, an eight-fold coordination, may occur, giving BVS of 0.91 and 1.16 v.u., respectively (0.86 and 1.14 v.u. in the present refinement). Following Ballirano (2015), a seven-fold coordination seems more likely, providing an overall charge neutrality to the crystal structure. In each unit cell there are four K^+ cations and eight SO_4 groups; consequently, in order to achieve a seven-fold coordination for all K^+ ions, a *k* value of 0.5 would be necessary. In Tl-bearing alum-(K) the *k* order parameter of 0.77 corresponds to 1.84 SO_4 groups available for bonding to K^+ through O(3)A, i.e., 46% and 54% of seven-fold and six-fold coordinated K sites, respectively. The

250 "average" K site would have a BVS of 0.71 v.u., a value still relatively low which confirms the
251 occurrence of another large cation, i.e., NH_4^+. Unfortunately, the quality of chemical data and the
252 small amount of available material did not allow to quantify the NH_4 content. Some hints can be
253 obtained from the crystal structure refinement. The refined site scattering at the K site is 26.4
254 electrons per formula unit (epfu). Chemical data indicate the occurrence of a deficit of cations at the
255 K site and spectroscopic data confirm the occurrence of $(NH_4)^+$. Assuming that the difference from
256 the full occupancy is represented by $(NH_4)^+$ ions, the site population $[K_{0.74}(NH_4)^+_{0.16}Tl_{0.10}]$ can be
257 proposed, corresponding to a site scattering of 23.3 epfu. Finally, the K site shows a relatively large
258 anisotropic displacement ellipsoid, with the longest axis in the direction of O(3)A. Consequently, a
259 slight shift towards O(3)A may occur, increasing its BVS.

260 In order to study the local environment of thallium within the crystal structure of alum-(K),
261 XAS studies were performed at the Tl L_3 edge on the "LISA" CRG beamline at ESRF (d'Acapito et
262 al., 2019). The XANES spectrum of alum-(K) is shown in Figure 4a, together with the spectra of
263 reference compounds. The position and shape of the main absorption edge confirms that Tl occurs
264 as Tl^+, with the XANES region fairly resembling that of Tl_2SO_4. Thallium L_3-edge EXAFS and
265 Fourier transform of measured samples are shown in Figures 4b and c, respectively, together with
266 the corresponding multiparameter fits; fit results are shown in Table 6. The spectrum was fitted
267 starting from the model obtained from the crystal structure refinement for the K site. Attempts to fit
268 the first coordination shell with only 6 O atoms were unsuccessful. Data were then satisfactorily
269 modelled introducing the short path corresponding to the Tl–O3(A) bond. In agreement with the
270 larger ionic radius, the short Tl–O bond has a distance of 2.66(2) Å, thus slightly higher than the
271 average K–O3(A) distance obtained from the crystal structure refinement. On the other hand, the
272 average six-fold Tl–O bond distance from EXAFS results significantly shorter than that observed in
273 the structural refinement [2.84(2) vs. 2.997(2) Å], thus extremely close to the ideal value of 2.835 Å
274 that would lead to a BVS of 1 v.u. for Tl in 6-fold coordination. This discrepancy may be related to
275 a locally higher value of the *k* disorder parameter around Tl atoms. The multiparameter fit results

highlight in any case that the contribution of the Tl–O3(A) bond is not negligible; the weak EXAFS signal however prevents us from obtaining an estimation of the probability for the short Tl–O3(A) path to occur. The second peak in the Fourier transform corresponds to a further Tl–O shell at 3.82(2) Å that can be interpreted as an interaction with the O(4) atoms of the SO_4 group in the more likely α orientation.

The BVS at O sites confirm the occurrence of H_2O groups at Ow(1) and Ow(2), and O^{2-} anions at O(3)/O(3)A and O(4)/O(4)A. The latter are acceptors of H-bonds from Ow(1) and Ow(2), the only exception being represented by O(3)A, which is not involved in any H-bond. Table 7 gives the geometrical features of H-bonds in the studied sample, agreeing with previous determinations (e.g., Nyburg et al. 2000). Micro-Raman spectrum of Tl-bearing alum-(K) (Fig. 3) shows a broad band in the O–H stretching region. Its deconvolution reveals the occurrence of at least four main bands, at 2916, 3176, 3381, and 3526 cm^{-1}. Using the relation proposed by Libowitzky (1999) between O–H stretching frequencies and O···O distances, the following distances can be calculated (in Å): 2.63, 2.70, 2.79, and 2.94, to be compared with the values given in Table 7. Since all H_2O groups are bonded to K or to Al, the chemical formula of alum-(K) should be correctly written as $KAl(SO_4)_2(H_2O)_{12}$.

Voltaite: crystal-chemistry and thallium speciation

Voltaite, $K_2Fe^{2+}{}_5Fe^{3+}{}_3Al(SO_4)_{12}\cdot 18H_2O$, is a member of the voltaite group, formed by cubic ($Fd\bar{3}c$) and tetragonal ($I4_1/acd$) species having general formula $X_2Y^{2+}{}_5Z^{3+}{}_3Al(TO_4)_{12}\cdot 18H_2O$, where $X = K^+$, $(NH_4)^+$, Tl^+, Rb^+; $Y = Fe^{2+}$, Mg^{2+}, Zn^{2+}, Mn^{2+}, Cd^{2+}, Co^{2+}; $Z = Fe^{3+}$; and $T = S^{6+}$. In some synthetic compounds, Al can be replaced by Fe^{3+}, e.g., in "K-Mg-Fe^{3+}-voltaite" described by Schwarte and Fischer (1989). In addition to voltaite, other natural members of this group are ammoniomagnesiovoltaite ($X = (NH_4)^+$, $Y = Mg^{2+}$), ammoniovoltaite ($X = (NH_4)^+$, $Y = Fe^{2+}$), magnesiovoltaite ($X = K^+$, $Y = Mg^{2+}$), and zincovoltaite ($X = K^+$, $Y = Zn^{2+}$). The group is completed by pertlikite, which shows a tetragonal superstructure owing to the ordering of divalent

cations (Ertl et al. 2008). Other compositions were synthesized (e.g., Gossner and Fell 1932; Gossner and Drexler 1933; Gossner and Besslein 1934).

Back-scattered electron images of voltaite from Fornovolasco revealed the occurrence of a complex chemical zoning (see Supplementary Material). The chemical formulae of the darker and brighter domains, recalculated on the basis of 66 O apfu, taking into account the data given in Table 1, are $(K_{1.91}Tl_{0.28})_{\Sigma 2.19}(Fe^{2+}_{3.48}Mg_{0.95}Mn_{0.63})_{\Sigma 5.06}Fe^{3+}_{3.07}Al_{0.98}S_{11.92}O_{48}\cdot 18H_2O$ and $(K_{2.04}Tl_{0.32})_{\Sigma 2.36}(Fe^{2+}_{3.83}Mg_{0.91}Mn_{0.29})_{\Sigma 5.03}Fe^{3+}_{3.05}Al_{0.97}S_{11.92}O_{48}\cdot 18H_2O$, respectively.

The crystal structure of voltaite group minerals, first solved by Mereiter (1972), can be described as a heteropolyhedral framework with cavities hosting disordered $Al(H_2O)_6$ octahedra (Fig. 5a). Indeed, Al is coordinated by six H_2O groups belonging to two distinct H_2O-hosting sites, i.e., Ow(6) and Ow(7). Each ordered Al-centered octahedron is formed by three H_2O groups belonging to Ow(6) and three belonging to Ow(7) (Fig. 5b).

The framework is formed by pinwheels centered at the $^{M(1)}Fe^{3+}O_6$ octahedra; the oxygen atoms belonging to this octahedron are shared with six SO_4 groups. The S site has an average <S–O> distance of 1.478 Å, with a corresponding BVS of 5.93 v.u. In agreement with Majzlan et al. (2013), each *M*(1) position is a point in the structure of voltaite where three kröhnkite-like heteropolyhedral chains intersect. The *M*(1) site is mainly occupied by Fe, in agreement with Majzlan *et al*. (2013), who reported a limited mixing between M^{2+} and M^{3+} cations in Fe^{2+}-Mg voltaites. Bond-valence sum (3.00 valence unit, v.u.) agrees with this occupancy. The slight increase in the average *M*(1)–O distance (2.014 Å), with respect to the expected value of 1.995 Å calculated using the ionic radii of $^{VI}Fe^{3+}$ and $^{II}O^{2-}$ given by Shannon (1976), assuming the full occupancy by Fe^{3+}, suggests the occurrence of Fe^{2+}. Neglecting minor Mg^{2+}, a site population $(Fe^{3+}_{0.87}Fe^{2+}_{0.13})$ can be proposed for *M*(1).

The *M*(2) site is coordinated by two H_2O groups, hosted at Ow(5), and four O^{2-} anions, and it shows an average <*M*(2)–φ> (where φ = O^{2-}, H_2O) distance of 2.055 Å. In agreement with the chemical data (taking into account the inhomogeneity of the studied crystals), and considering the

heterovalent substitution $^{M(1)}Fe^{3+} + {}^{M(2)}Fe^{2+} = {}^{M(1)}Fe^{2+} + {}^{M(2)}Fe^{3+}$, the idealized site population should be $(Fe^{2+}_{3.3}Fe^{3+}_{1.3}Mg_{1.0}Mn_{0.4})_{\Sigma 6}$. This site population corresponds to 141.6 electrons per formula unit (epfu), to be compared with the refined site occupancy, giving 135 epfu. This discrepancy (1.3 electron per site) is likely due to the chemical variability of the studied crystals. The bond-valence sum, 2.52 v.u., is larger than the expected value of 2.22 v.u. The Fe^{2+}/Fe^{3+} atomic ratio calculated on the basis of electron microprobe analysis agrees with the results of Mössbauer spectroscopy. The spectrum of voltaite could be accurately fitted with one Fe^{2+} and one Fe^{3+} doublet (Fig. 6). In agreement with Dyar *et al*. (2013), the observed doublets can be assigned to ferrous and ferric iron in octahedral coordination. The isomer shifts and the quadrupole splitting for the Fe^{2+} doublet were found at 1.31 mm/s and 1.78 mm/s, respectively. The Fe^{3+} doublet shows an isomer shift of 0.46 mm/s and a quadrupole splitting of 0.33 mm/s. These data are in accord with those reported for the synthetic sample $Fe_{40}Mg_{60}$ of voltaite by Majzlan et al. (2013) and for ammoniovoltaite (Zhitova et al. 2018). With the assumption of similar recoil-free fractions, the Mössbauer spectrum of voltaite from Fornovolasco indicates an atomic ratio Fe^{2+}/Fe_{tot} of 0.55, to be compared with 0.53 and 0.56 calculated for the darker and brighter domains observed in BSE images.

The K site has six oxygen atoms at 2.875(4) Å, and six additional very long (i.e., very weak) bonds, at 3.276(5) Å. These values can be compared with those of synthetic $K_2Fe^{2+}_5Fe^{3+}_3Al(SO_4)_{12}\cdot 18H_2O$, i.e., 2.886 and 3.293 Å, respectively. The refined site scattering agrees with chemical data, confirming a minor replacement of K by Tl. The crystal structure refinement points to a Tl/(Tl+K) atomic ratio of 0.06, to be compared with 0.13 – 0.14 observed through electron microprobe analyses. Actually, the occurrence of minor NH_4^+ also replacing K^+ could explain the lower observed site scattering at the K site with respect to that calculated on the basis of electron microprobe data. The occurrence of Tl in voltaite was also confirmed through XAS. As in alum-(K), the position and shape of the main absorption edge confirm that Tl is present as Tl^+. Quantitative EXAFS analysis (Table 6) shows that the local structure around Tl is in substantial agreement with the results of the single-crystal X-ray diffraction refinement, with Tl

354 bonding ~ 6 O atoms at ~ 2.9 Å. The second shell is represented by six S atoms at ~ 3.6 Å. No hints
355 of the longer Tl–O interaction at ~ 3.3 Å can be inferred from EXAFS data. The moderate misfit
356 between data and fit in voltaite may be ascribed to the high degree of disorder of the structure;
357 EXAFS provides an average information and it is therefore difficult to model disordered structures
358 such as that of voltaite, especially with respect to coordination shells higher than the first.

359 Thallium-rich or thallium-bearing members of the voltaite group are mainly known as
360 synthetic products, e.g., "Tl-Fe voltaite", "Tl-Mg voltaite", and "Tl-Cd voltaite" obtained by
361 Gossner and Fell (1932). Manilici et al. (1965) and later Götz et al. (1968) described a hydrated
362 potassium thallium sulfate, with Tl supposed as Tl^{3+}, and named it "monsmedite". This mineral had
363 morphology, optical properties, as well as the X-ray powder diffraction pattern very similar to those
364 shown by voltaite group minerals. Indeed, a reexamination of this mineral by Zemann (1993), Johan
365 et al. (2009), and Kovács-Pálffy et al. (2011) proved that "monsmedite" is voltaite with up to ~ 7.5
366 wt% Tl_2O. Its unit-cell parameter, a = 27.2587 Å (Kovács-Pálffy et al. 2011), is larger than that of
367 synthetic $K_2Fe^{2+}{}_5Fe^{3+}{}_3Al(SO_4)_{12}\cdot 18H_2O$ (a = 27.234 Å – Mereiter 1972) and can be compared with
368 that observed for Tl-bearing voltaite studied in this work, i.e., a = 27.2635(18) Å.

369 In addition, Kovács-Pálffy et al. (2011) discussed the chemical zoning of Tl-bearing voltaite,
370 showing an increase in the Tl content from the core to the rim of the studied crystal. X-ray maps
371 collected on the specimen from Fornovolasco showed a similar zoning (See Supplementary
372 Material). Such a chemical zoning is likely related to the relatively large estimated standard
373 deviation (e.s.d.) of unit-cell parameter; as pointed out by Majzlan et al. (2013), the e.s.d. on the
374 lattice parameters of voltaite are always one or two orders of magnitude higher than those of
375 associated minerals, despite the euhedrality of voltaite (Fig. 1). X-ray maps show that both K and Tl
376 increase from the core to the rim of the studied crystals, whereas the only detected element enriched
377 in the core seems to be represented by Mn. Actually, the sum (K + Tl) is overestimated in electron
378 microprobe analyses (sum of 2.19 and 2.36 apfu); such an excess was found also in several analyses
379 reported by Majzlan et al. (2013) (up to 2.56 K per formula unit, with an average, among the

studied samples of 2.17 K atoms per formula unit). It seems likely that the depletion of K and Tl in the core of the studied crystals may be related to the occurrence of NH_4^+. Nitrogen was indeed detected in electron microprobe analysis but not quantified, and the characteristic band at 1428 cm^{-1} was observed in the FTIR spectrum of Tl-bearing voltaite (Fig. 7a). Majzlan et al. (2013) discussed the infrared spectra of selected samples of synthetic voltaites. Only NH_4-bearing samples show a band at 1431 cm^{-1}, related to the ν_3 mode of the NH_4 group. Similarly, Szakáll et al. (2012) and Zhitova et al. (2019) reported such a band in the FTIR spectra of ammoniomagnesiovoltaite (1431 cm^{-1}) and ammoniovoltaite (1433 cm^{-1}), respectively. Moreover, Košek et al. (2019) reported a band at 1428 cm^{-1} in the Raman spectrum of voltaite from the Anna I dump, Aldsdorf (Germany). Figure 7b shows the Raman spectrum of voltaite from Fornovolasco. No band at such a position can be observed. This is not surprising; for instance, in the Raman spectra of the NH_4-sulfates carlsonite and huizingite-(Al), the occurrence of NH_4 groups was not detected in the latter and only a very weak and broad band was observed in the former. On the contrary, FTIR clearly showed the presence of this constituent (Kampf et al. 2016).

As in previous refinements, only the H atoms bonded to Ow(5) have been located. Ow(5) is donor in two H-bonds with O(2) and O(3) (Table 6), both belonging to an (SO_4) group. In addition, every O atom hosted at O(3) is acceptor of H-bond from Ow(6) or Ow(7). Ow(6) is donor of H-bonds to two distinct oxygen atoms hosted at two symmetry-related O(3) sites, with Ow(6)···O(3) distances of 2.47 and 2.58 Å, respectively. An O···O distance of 2.47 Å is very short, being shorter than the shortest distances reported by Ferraris and Franchini-Angela (1972). However, similar distances have been reported in previous refinements of the crystal structure of voltaite group minerals (e.g., Mereiter 1972; Ertl et al. 2008), as well as in other phases, e.g., in libethenite and zincolibethenite, in which H-bonds characterized by O···O distances of 2.48 and 2.47 Å were reported, respectively (Cordsen 1978; Williams et al. 2006). Similarly, Ow(7) is donor of H-bonds to two oxygen atoms hosted at O(3), with O···O distances of 2.77 and 2.82 Å. Consequently, owing to the positional disorder affecting the Al-centered octahedra, O(3) can be involved in different H-

bond configurations. It is worth noting that O(3) is acceptor of only one H-bond from Ow(6) or Ow(7); taking into account also the H-bond accepted from Ow(5), the BVS at O(3) ranges between 1.89 and 2.11 v.u. The oxygen atoms at Ow(6) and Ow(7), being donor of H-bonds, have a corrected BVS of -0.14 and +0.13 v.u., respectively.

The FTIR spectrum of Tl-bearing voltaite (Fig. 7a) shows strong and broad absorption bands in the range 3900 – 2900 cm^{-1}, related to the O–H stretching modes of H_2O groups centered around 3573, 3448, 3250, and 3102 cm^{-1}. Two distinctive bands at 1688 and 1638 cm^{-1} can be attributed to the bending of H_2O groups. Applying the relation of Libowitzky (1999), the following distances can be calculated (in Å): 2.67, 2.72, 2.84, and 3.10 Å. Indeed, the short O(3)···Ow(6) are likely the result of the average position of Ow(6), affecting the actual position of O(3), as indicated by the relatively high U_{eq} value, the highest among O atoms in voltaite, in agreement with Mereiter (1972).

Since all H_2O groups are bonded to K, Al, or *M* sites, the chemical formula of voltaite should be correctly written as $K_2Fe^{2+}_5Fe^{3+}_3Al(SO_4)_{12}(H_2O)_{18}$.

Implications

Sulfate mineral assemblages play an important role in the storage and transport of acids and potentially toxic and bioavailable metals released during the weathering of ore deposits, coals, and mine wastes (Jambor et al. 2000). Therefore, as stressed by several authors (e.g., Jamieson, 2011; Nordstrom, 2011), the characterization of the mineralogy and geochemistry of oxidation products is crucial for predicting their environmental impact and the solid-phase controls on dissolved metal concentration. This characterization involves the accurate knowledge of the crystal-chemistry of sulfate minerals, a goal that can be achieved only through a multi-technique approach, integrating chemical, structural, and spectroscopic data.

Thallium can be a minor to trace elements occurring in several ore deposits and representing a potential environmental hazard (e.g., Xiao et al. 2004). However, this element can be overlooked and its occurrence could be revealed, for instance, through the accurate study of secondary mineral

assemblages. Previous geochemical studies (e.g., Vlasov 1966) highlighted a complex behavior shown by Tl in the oxidation zone that can be summarized in four stages:

1) thallium is usually removed and it does not appear in the common sulfates forming during the earliest stages of sulfides oxidation. Taking into account pyrite oxidation, this stage may correspond to the crystallization of Fe^{2+} and mixed Fe^{2+}/Fe^{3+} species (e.g., Jambor et al. 2000);

2) the content of thallium can increase following the crystallization of alunite group minerals (e.g., jarosite). This stage corresponds to the latest stage of sulfate crystallization, preceding the formation of iron oxy-hydroxides (e.g., Jambor et al. 2000);

3) when iron oxy-hydroxides are formed, thallium-bearing species are usually dissolved and removed again;

4) finally, thallium can be oxidized from Tl^{+} to Tl^{3+}, forming the virtually insoluble mineral avicennite.

The mineralogy of thallium in secondary environments in limited to very few species. Avicennite, Tl_2O_3 (Karpova et al. 1958; Radke et al. 1978), is the only known Tl^{3+} oxide and it is usually found in deeply altered occurrences (e.g., Buus, Switzerland; Herrmann et al. 2018). As reported in the introduction, the three Tl^{+}-oxysalts dorallcharite (Balić-Žunić et al. 1994), lanmuchangite (Chen and Wang 2001), and thalliumpharmacosiderite (Rumsey et al. 2014) are the other known species. Dorallcharite is the Tl-analogue of jarosite and crystallizes during stage (2). On the contrary, lanmuchangite is associated, at its type locality, with melanterite, pickeringite, alum-(K), jarosite, and gypsum (Chen and Wang 2001), and it belongs to stage (1). No information about the occurrence of thalliumpharmacosiderite (Rumsey et al. 2014) is available, as the publication is still pending. However, bariopharmacosiderite was observed in the deeply oxidized assemblage of Buus (Herrmann et al. 2018) and likely its thallium-analogue could be a mineral formed during the latest stages of ore weathering. In addition, it is well known that Tl^{+} can occur in soils, being hosted in micaceous phyllosilicates (e.g., illite; Herrmann et al. 2018), and can occur as

457 Tl^{+} or Tl^{3+} in Mn oxides. Likely, this could be the genesis of the recently approved mineral
458 thalliomelane, $TlMn^{4+}_{7.5}Cu^{2+}_{0.5}O_{16}$ (Gołębiowska et al. 2019).

459 The description of thallium-bearing sulfates from the Fornovolasco mining complex,
460 representing an early assemblage in the oxidation of Tl-bearing pyrite ores, suggests that thallium
461 can be transiently sequestered by potassium sulfates during the first stages of weathering, promoting
462 its change of speciation, from a trace element in pyrite ores (up to 1110 μg/g – D'Orazio et al.
463 2017) to a major constituent of secondary assemblages, achieving concentrations up to some weight
464 unit per cent. This behavior disagrees with the description given above (Vlasov 1966). In our
465 opinion, this disagreement could be due the occurrence of K-rich phases in the early stages of
466 oxidation, that could promote the thallium concentration in crystallizing sulfates; in other K-poor
467 environments, where alum-(K) and voltaite do not crystallize, it is very likely that the thallium
468 behavior may follow the behavior described by Vlasov (1966). In addition, it seems likely that the
469 Tl-enrichment occurs late during the first stage of oxidation. The present study, as well as previous
470 contributions (e.g., Kovács-Pálffy et al. 2011), suggest that Tl is enriched during the final stages of
471 the crystal growth of Tl-bearing sulfates, as exemplified by the Tl-enriched rims of voltaite. This
472 could have an environmental significance, as the partial dissolution of voltaite crystals may be
473 sufficient to release high amounts of Tl in water, since this element is more concentrated in the
474 outer rims of the crystals.

475 The occurrence of thallium is usually neglected and this could also be due to analytical
476 difficulties. For instance, a routinary EDS analysis may fail to detect the occurrence of minor Tl,
477 owing to the interference between Tl*M*α and S*K*α lines. This study shows that, in the case of alum-
478 (K), Raman spectroscopy could reveal the substitution of K^{+} by larger cations; if FTIR spectroscopy
479 does not reveal the occurrence of N–H vibrational modes, then Tl could be a good candidate for
480 being the K-substituent.

481 As alum-(K) and voltaite are among the more common K-bearing minerals in sulfate
482 assemblages occurring in weathered pyrite ore deposits, their crystal-chemistry can dramatically

483 influence the composition of water draining for these areas. Indeed, they could play a central role in
484 storing and temporarily sequestering Tl, acting as scavengers of this element in acid mine drainage
485 systems. During dry conditions, Tl is sequestered and hosted in the crystal structure of these
486 potassium sulfates. On the contrary, during the wet season or flood events, sulfate assemblages can
487 be partially or totally dissolved, contributing pulses of potentially bioavailable metals and
488 metalloids (among which Tl) in the hydrosphere. Consequently, a good knowledge of the crystal-
489 chemistry of alum-(K) and voltaite gives additional useful information to understand the processes
490 related to acid mine drainage systems.
491

492 ## Acknowledgments

493 This research received support from the Ministero dell'Istruzione, dell'Università e della Ricerca
494 through the projects SIR 2014 “THALMIGEN – Thallium: Mineralogy, Geochemistry, and
495 Environmental Hazards” (Grant No. RBSI14A1CV) and from the University of Pisa through the
496 project P.R.A. 2018-2019 “Georisorse e Ambiente” (Grant No. PRA_2018_41). The University
497 Centrum for Applied Geosciences (UCAG) is thanked for the access to the Eugen F. Stumpfl
498 electron microprobe laboratory of Leoben (Austria). XAS measurements were performed during
499 experiment 08-01-1016 and in-house beamtime, Francesco d’Acapito and LISA staff members are
500 thanked for the provision of the beamtime. The paper benefited of the constructive comments by
501 Igor Pekov and two anonymous reviewers.

502 **References**

503 Ankudinov, A.L., Ravel, B., Rehr, J.J., and Conradson, S.D. (1998) Real-space multiple-scattering
504 calculation and interpretation of X-ray absorption near-edge structure. Physical Review, B58,
505 7565-7576.
506 Balić-Žunić, T., Moëlo, Y., Lončar, Z., and Micheelsen, H. (1994) Dorallcharite,
507 $Tl_{0.8}K_{0.2}Fe_3(SO_4)_2(OH)_6$, a new member of the jarosite-alunite family. European Journal of
508 Mineralogy, 6, 255-263.

509 Ballirano, P. (2015) Thermal behaviour of alum-(K) $KAl(SO_4)_2 \cdot 12H_2O$ from in situ laboratory
510 high-temperature powder X-ray diffraction data: thermal expansion and modelling of the
511 sulfate orientational disorder. Mineralogical Magazine, 79, 157-170.
512 Beevers, C.A., and Lipson, H. (1934) Crystal structure of the alums. Nature, 134, 327-327.
513 Biagioni, C., Bonaccorsi, E., and Orlandi, P. (2011) Volaschioite, $Fe^{3+}_4(SO_4)O_2(OH)_6 \cdot 2H_2O$, a new
514 mineral species from Fornovolasco, Apuan Alps, Tuscany, Italy. Canadian Mineralogist, 49,
515 605-614.
516 Biagioni, C., D'Orazio, M., Vezzoni, S., Dini, A., and Orlandi, P. (2013) Mobilization of Tl-Hg-As-
517 Sb-(Ag,Cu)-Pb sulfosalt melts during low-grade metamorphism in the Alpi Apuane (Tuscany,
518 Italy). Geology, 41, 747-750.
519 Biagioni, C., D'Orazio, M., Lepore, G.O., d'Acapito, F., and Vezzoni, S. (2017) Thallium-rich rust
520 scales in drinkable water distribution systems: A case study from northern Tuscany, Italy.
521 Science of the Total Environment, 587-588, 491-501.
522 Brese, N.E., and O'Keeffe, M. (1991) Bond-valence parameters for anion-anion bonds in solids.
523 Acta Crystallographica, B48, 152-154.
524 Bruker AXS Inc. (2004) APEX 2. Bruker Advanced X-ray Solutions, Madison, Wisconsin, USA.
525 Chen, D., and Wang, G. (2001) A new mineral – lanmuchangite. Acta Mineralogica Sinica, 21,
526 271-277.
527 Cordsen, A. (1978) A crystal-structure refinement of libethenite. Canadian Mineralogist, 16, 153-
528 157.
529 Cork, J.M. (1927) The crystal structure of some of the alums. Philosophical Magazine, 4, 688-698.
530 Craw, D. (1981) Oxidation and microprobe-induced potassium mobility in iron-bearing
531 phyllosilicates from the Otago schists, New Zealand. Lithos, 14, 49-57.
532 d'Acapito, F., Trapananti, A., Torrengo, S., and Mobilio, S. (2014) X-ray absorption spectroscopy:
533 the Italian beamline GILDA at the ESRF. Notiziairio Neutroni e Luce di Sincrotrone, 19, 14.

d'Acapito, F., Lepore, G.O., Puri, A., Laloni, A., La Mannna, F., Dettona, E., De Luisa, A., and Martin, A. (2019) The LISA beamline at ESRF. Journal of Synchrotron Radiation, 26, 551-558.

D'Orazio, M., Biagioni, C., Dini, A., and Vezzoni, S. (2017) Thallium-rich pyrite ores from the Apuan Alps, Tuscany, Italy: constraints for their origin and environmental concerns. Mineralium Deposita, 52, 687-707.

Ertl, A., Dyar, M.D., Hughes, J.M., Brandstätter, F., Gunter, M.E., Prem, M., and Peterson, R.C. (2008) Pertlikite, a new tetragonal Mg-rich member of the voltaite group from Madeni Zakh, Iran. The Canadian Mineralogist, 46, 661-669.

Ferraris, G. and Franchini-Angela, M. (1972) Survey of the geometry and environment of water molecules in crystalline hydrates studied by neutron diffraction. Acta Crystallographica, B28, 3572-3583.

Ferraris, G., and Ivaldi, G. (1988) Bond valence vs bond length in O···O hydrogen bonds. Acta Crystallographica, B44, 341-344.

Frost, R.L., and Kloprogge, J.T. (2001) Raman microscopy study of kalinite, tschermigite and lonecreekite at 298 and 77 K. Neues Jahrbuch für Mineralogie, Monatshefte, 2001, 27-40.

George, L.L., Biagioni, C., D'Orazio, M. and Cook, N.J. (2018) Textural and trace element evolution of pyrite during greenschist facies metamorphic recrystallization in the southern Apuan Alps (Tuscany, Italy): Influence on the formation of Tl-rich sulfosalt melt. Ore Geology Reviews, 102, 59-105.

Ghezzi, L., D'Orazio, M., Doveri, M., Lelli, M., Petrini, R., and Giannecchini, R. (2019) Groundwater and potentially toxic elements in a dismissed mining area: Thallium contamination of drinking spring water in the Apuan Alps (Tuscany, Italy). Journal of Geochemical Exploration, 197, 84-92.

558 Gołębiowska, B., Pieczka, A., Zubko, M., Voegelin, A., Göttlicher, J., and Rzepa, G. (2019)
559 Thalliomelane, IMA 2019-055. CNMNC Newsletter No. 52, Mineralogical Magazine, 83,
560 https://doi.org/10.1180/mgm.2019.73.
561 Gossner, B., and Besslein, J. (1934) Hydrated sulfates of three metals. Centralblatt für Mineralogie,
562 Geologie, und Paläontologie, 1934A, 358-364 (in German).
563 Gossner, B., and Drexler, K. (1933) Structural and molecular units of sulfates of the voltaite type.
564 Centralblatt für Mineralogie, Geologie, und Paläontologie, 1933A, 83-91 (in German).
565 Gossner, B., and Fell, E. (1932) Beitrag zur Kenntnis voltait-artiger Sulfate. Berichte der deutschen
566 chemischen Gesellschaft, 65B, 393-395.
567 Götz, A., Mihalka, St., Ionita, I., and Toth, Z. (1968) Monsmeditul – un nuo mineral de taliu de la
568 Baia Sprie. Revista Mineralor, 19, 154-159.
569 Grice, J.D., and Ferraris, G. (2003) New minerals approved in 2002 and nomenclature
570 modifications approved in 1998-2002 by the Commission on New Minerals and Mineral
571 Names, International Mineralogical Association. Canadian Mineralogist, 41, 795-802.
572 Hawthorne, F.C., Krivovichev, S.V., and Burns, P.C. (2000) The crystal chemistry of sulfate
573 minerals. Reviews in Mineralogy and Geochemistry, 40, 1-101.
574 Herrmann, J., Voegelin, A., Palatinus, L., Mangold, S., and Majzlan, J. (2018) Secondary Fe-As-Tl
575 mineralization in soils near Buus in the Swiss Jura Mountains. European Journal of
576 Mineralogy, 30, 887-898.
577 Jambor, J.L., Nordstrom, D.K., and Alpers, C.N. (2000) Metal-sulfate salts from sulfide mineral
578 oxidation. Reviews in Mineralogy and Geochemistry, 40, 303-350.
579 Jamieson, H.E. (2011) Geochemistry and mineralogy of solid mine waste: essential knowledge for
580 predicting environmental impact. Elements, 7, 381-386.
581 Johan, Z., Udubasa, G., and Zemann, J. (2009) “Monsmedite”, a discredited potassium thallium
582 sulphate mineral from Baia Sprie and its identity with voltaite: The state of the art. Neues
583 Jahrbuch für Mineralogie, Abhandlungen, 186, 63-66.

584 Karpova, K.N., Kon'kova, E.A., Larkin, E.D., and Savel'ev, V.F. (1958) Avicennite – a new
585 mineral. Doklady Akademii Nauk Uzbekskoi SSR, 2, 23-26 (in Russian).
586 Košek, F., Edwards, H.G.M., and Jehlička, J. (2019) Raman spectroscopic vibrational analysis of
587 the complex iron sulfates clairite, metavoltine, and voltaite from the burning coal dump Anna
588 I, Alsdorf, Germany. Journal of Raman Spectroscopy, 2019, 1-8.
589 Kovács-Pálffy, P., Muske, J., Földvári, M., Kónya, P., Homonnay, Z., Ntaflos, T., Papp, G., Király,
590 E., Sajó, I., Szilágyi, V., and Boszó, G. (2011) Detailed study of "monsmedite" specimens
591 from the original (1963) find, Baia Sprie, Baia Mare Ore District (Romania). Carpathian
592 Journal of Earth and Environmental Sciences, 6, 321-330.
593 Larson, A.C., and Cromer, D.T. (1967) Refinement of the alum structures. III. X-ray study of the α
594 alums, K, Rb and $NH_4Al(SO_4)_2 \cdot 12H_2O$. Acta Crystallographica, 22, 793-800.
595 Lee, P.A., Citrin, P.H., Eisenberger, P.T., and Kincaid, B.M. (1981) Extended X-ray absorption fine
596 structure – its strengths and limitations as a structural tool. Reviews of Modern Physics, 53,
597 769-806.
598 Libowitzky, E. (1999) Correlation of O–H stretching frequencies and O–H···O hydrogen bond
599 lengths in minerals. Monatshefte für Chemie, 130, 1047-1059.
600 Lipson, H. (1935) The relation between the alum structures. Proceedings of the Royal Society of
601 London, Series A, Mathematical and Physical Sciences, 151, 347-356.
602 Kampf, A.R., Richards, R.P., Nash, B.P., Murowchick, J.B., and Rakovan, J.F. (2016) Carlsonite,
603 $(NH_4)_5Fe^{3+}{}_3O(SO_4)_6 \cdot 7H_2O$, and huizingite-(Al), $(NH_4)_9Al_3(SO_4)_8(OH)_2 \cdot 4H_2O$, two new
604 minerals from a natural fire in an oil-bearing shale near Milan, Ohio. American Mineralogist,
605 101, 2095-2107.
606 Majzlan, J., Schlicht, H., Wierzbicka-Wieczorek, M., Giester, G., Pöllmann, H., Brömme, B.,
607 Doyle, S., Buth, G., and Koch, C.B. (2013) A contribution to the crystal chemistry of the
608 voltaite group: solid solutions, Mössbauer and infrared spectra, and anomalous anisotropy.
609 Mineralogy and Petrology, 107, 221-233.

610 Manilici, V., Giusca, D., and Stiopol, V. (1965) Studiul zacamintului de la Baia Sprie (Reg. Baia
611 Mare). Memoriile Comitetului Geologic, 7, 1-113.
612 Martini, J.E.J. (1983) Lonecreekite, sabieite and clairite, new secondary ammonium ferric iron
613 sulphates from Lone Creek Fall Cave, near Sabie, eastern Transvaal. Annals of the Geological
614 Survey of South Africa, 17, 29-34.
615 Mereiter, K. (1972) Die Kristallstruktur des Voltaits, $K_2Fe^{2+}{}_5Fe^{3+}{}_3Al[SO_4]_{12}\cdot 18H_2O$. Tschermaks
616 Mineralogische und Petrographische Mitteilungen, 18, 185-202.
617 Nordstrom, D.K. (2011) Mine waters: acidic to circumneutral. Elements, 7, 393-398.
618 Nyburg, S.C., Steed, J.W., Aleksovska, S., and Petruševski, V.M. (2000) Structure of the alums. I.
619 On the sulfate group disorder in the α-alums. Acta Crystallographica, B56, 204-209.
620 Perotti, M., Petrini, R., D'Orazio, M., Ghezzi, L., Giannecchini, R., and Vezzoni, S. (2018)
621 Thallium and other potentially toxic elements in the Baccatoio stream catchment (Northern
622 Tuscany, Italy) receiving drainages from abandoned mines. Mine Water Environment, 37,
623 431-441.
624 Prescher, C., McCammon, C., and Dubrovinsky, L. (2012) MossaA: a program for analyzing
625 energy-domain Mössbauer spectra from conventional and synchrotron sources. Journal of
626 Applied Crystallography, 45, 329–331.
627 Puri, A., Lepore, G. O., and d'Acapito, F. (2019) The New Beamline LISA at ESRF: Performances
628 and Perspectives for Earth and Environmental Sciences. Condensed Matter, 4, 12.
629 Radtke, A.S., Dickson, F.W., and Slack, J.F. (1978) Occurrence and formation of avicennite, Tl_2O_3,
630 as a secondary mineral at the Carlin gold deposit, Nevada. Journal of Research USGS, 6, 241-
631 246.
632 Ravel, B. (2001) ATOMS: crystallography for the X-ray absorption spectroscopist. Journal of
633 Synchrotron Radiation, 8, 314-316.
634 Ravel, B., and Newille, M. (2005) ATHENA, ARTEMIS, HEPHAESTUS: data analysis for X-ray
635 absorption spectroscopy using IFEFFIT. Journal of Synchrotron Radiation, 12, 537-541.

636 Roberts, A.C., Venance, K.E., Seward, T.M., Grice, J.D. and Paar, W.H. (2006) Lafossaite, a new
637 mineral from the La Fossa crater, Vulcano, Italy. Mineralogical Magazine, 37, 165-168.
638 Rumsey, M.S., Mills, S.J., Spratt, J., Hay, D.G., and Farber, G. (2014) Thalliumpharmacosiderite,
639 IMA 2013-124. CNMNC Newsletter No. 20, June 2014, page 553; Mineralogical Magazine,
640 78, 549-558.
641 Schwarte, C., and Fischer, W. (1989) Zur Kristallstruktur des K-Mg-Fe-Voltaits. Zeitschrift für
642 Kristallographie, 186, 272-273.
643 Shannon, R.D. (1976) Revised effective ionic radii and systematic studies of interatomic distances
644 in halides and chalcogenides. Acta Crystallographica, A32, 751-767.
645 Sheldrick, G.M. (2015) Crystal structure refinement with SHELXL. Acta Crystallographica, C71,
646 3-8.
647 Szakáll, S., Sajó, I., Fehér, B., and Bigi, S. (2012) Ammoniomagnesiovoltaite, a new voltaite-
648 related mineral species from Pécs-Vasas, Hungary. The Canadian Mineralogist, 50, 65-72.
649 van der Pluijm, B., Lee, J.H., and Peacor, D.R. (1988) Analytical electron microscopy and the
650 problem of potassium diffusion. Clays and Clay Minerals, 36, 498-504.
651 Vlasov, K.A. (ed.) (1966) Geochemistry and mineralogy of rare elements and genetic types of
652 deposits. Vol. 1. Geochemistry of rare elements. Israel Program for Scientific Translations,
653 491-524.
654 Williams, P.A., Leverett, P., Birch, W.D., Hibbs, D.E., Kolitsch, U., and Mihajlovic, T. (2006)
655 Zinc-rich zincolibethenite from Broken Hill, New South Wales. Australian Journal of
656 Mineralogy, 12, 3-7.
657 Wilson, A.J.C. (1992) International Tables for Crystallography Volume C. Kluwer, Dordrecht.
658 Wojdyr, M. (2010) Fityk: a general-purpose peak fitting program. Journal of Applied
659 Crystallography, 43, 1126-1128.
660 Xiao, T., Guha, J., Boyle, D., Liu, C.-Q., Zheng, B., Wilson, G.C., Rouleau, A., and Chen, J. (2004)
661 Naturally occurring thallium: a hidden geoenvironmental health hazard? Environment

662 International, 30, 501-507.

663 Zemann, J. (1993) What is monsmedite? Romanian Journal of Mineralogy, 76, 97-98.

664 Zhitova, E.S., Siidra, O.I., Belakovsky, D.I., Shilovskikh, V.V., Nuzhdaev, A.A., and Ismagilova,
665 R.M. (2018) Ammoniovoltaite, $(NH_4)_2Fe^{2+}_5Fe^{3+}_3Al(SO_4)_{12}(H_2O)_{18}$, a new mineral from the
666 Severo-Kambalny geothermal field, Kamchatka, Russia. Mineralogical Magazine, 82, 1057-
667 1077.

668 Zhitova, E.S., Sergeeva, A.V., Nuzhdaev, A.A., Krzhizhanovskaya, M.G., and Chubarov, V.M.
669 (2019) Tschermigite from thermal fields of southern Kamchatka: high-temperature
670 transformation and peculiarities of IR-spectrum. Proceedings of the Russian Mineralogical
671 Society, 148, 100-116.

672

Table captions

Table 1 – Chemical data for alum-(K) and voltaite from the Fornovolasco mining complex.

Table 2 – Crystal data and summary of parameters describing data collection and refinement for alum-(K) and voltaite.

Table 3 – Site occupancy factors (s.o.f.), fractional atom coordinates, and isotropic (*) or equivalent isotropic displacement parameters (in $Å^2$) for alum-(K) and voltaite. U_{eq} is defined as one third of the trace of the orthogonalized U^{ij} tensor.

Table 4 – Selected bond distances (in Å) for alum-(K) and voltaite.

Table 5 – Weighted bond valences for alum-(K) and voltaite, in valence units (v.u.).

Table 6 – EXAFS multiparameter fit details for alum-(K) and voltaite, Tl L_3-edge

Table 7 – Bond lengths (Å), angles (°), and bond strengths (v.u.) for H-bonds in alum-(K) and voltaite.

Figure captions

Fig. 1 – Tl-bearing sulfates from the Fornovolasco mining complex. (a) Alum-(K) as colorless crystalline masses associated with römerite, copiapite, and minor voltaite. (b) Voltaite, {100} individuals with minor {111} and {110} faces, associated with a tabular crystal of alunogen.

Fig. 2 – Crystal structure of alum-(K), as seen down **a**, and the two different SO_4 configurations, not bonded (b) and bonded to K^+ (c). Dark grey and grey polyhedra represent Al and S sites, respectively. Dark grey, grey, and light grey small circles represent O, H, and Ow sites, respectively, whereas the K site is shown as large dark grey circles.

Fig. 3 – Micro-Raman (a) and FTIR (b) spectra of alum-(K) and band interpretation. The deconvolution of the O–H stretching region and the ν_1 (SO_4) modes in the Raman spectrum are shown on upper left and right in (a), respectively.

Fig. 4 – a) Normalized Tl-L_3 edge XANES for alum-(K), voltaite and model compounds. Tl L_3 edge EXAFS (b) and Fourier transform (c) of voltaite and alum-K. Black lines are data, open squares are fits.

Fig. 5 – Crystal structure of voltaite, as seen down **a** (a). Polyhedra: dark grey = *M*(1) site; grey = *M*(2) site; light grey = S site. Small circles: dark grey = Al site; light grey = O atoms bonded to H atoms, forming H_2O groups; grey = O atoms. Large dark grey circles = K site. The disordered H_2O groups around Al atoms are shown. Hydrogen atoms are not shown. In (b), an ordered Al-centered octahedron is shown down [111], along with the H-bond system. Same symbols as in (a), with the exception of Ow(6) and Ow(7) sites, shown as grey and black circles, respectively. Dashed lines represent H-bonds.

Fig. 6 – Mössbauer spectrum of voltaite obtained at room-temperature. Fitted absorption doublets assigned to Fe^{2+} and Fe^{3+} are indicated by dashed and dotted lines, respectively. Diamonds denote measured spectrum and black curve represents summed fitted doublets.

Fig. 7 –FTIR (a) and Raman (b) spectra of voltaite and band interpretation.

Supplementary material – Backscattered electron image (BSE) and X-ray maps of Tl-bearing voltaite.

This is a preprint, the final version is subject to change, of the American Mineralogist (MSA)
Cite as Authors (Year) Title. American Mineralogist, in press.
DOI: https://doi.org/10.2138/am-2020-7320

716 **Table 1** – Chemical data for alum-(K) and voltaite from the Fornovolasco mining complex.

	Alum-(K)*	Voltaite			Voltaite		
		Dark (n = 15)			Bright (n = 5)		
Oxide	wt%	wt%	range	e.s.d.	wt%	range	e.s.d.
SO_3	33.27	46.35	45.03 – 46.84	0.48	45.98	45.30 – 46.86	0.66
Al_2O_3	8.79	2.43	2.34 – 2.54	0.06	2.39	2.32 – 2.46	0.06
FeO_{tot}	-	22.85	22.14 – 23.95	0.63	23.83	23.47 – 24.21	0.32
Fe_2O_3	2.24	11.90			11.74		
FeO	-	12.14			13.27		
MgO	-	1.86	1.34 – 2.30	0.28	1.77	1.48 – 1.99	0.20
MnO	-	2.18	1.59 – 2.53	0.24	0.98	0.82 – 1.20	0.16
K_2O	7.13	4.36	3.19 – 5.23	0.44	4.62	4.27 – 5.12	0.31
Tl_2O	4.42	2.88	2.39 – 3.39	0.29	3.30	2.83 – 3.86	0.41
H_2O_{calc}	44.15	15.74			15.62		
Total	100.00	99.84			99.67		

717 Note: H_2O calculated on the basis of stoichiometry. In the chemical analyses of voltaite, the FeO
718 and Fe_2O_3 contents were calculated in order to match the atomic ratio $(Mg + Mn + Fe^{2+})/(Al + Fe^{3+})$
719 = 5/4.
720 *Normalized to total = 100 wt%.
721

This is a preprint, the final version is subject to change, of the American Mineralogist (MSA)
Cite as Authors (Year) Title. American Mineralogist, in press.
DOI: https://doi.org/10.2138/am-2020-7320

722 **Table 2** – Crystal data and summary of parameters describing data collection and refinement for

723 alum-(K) and voltaite.

Crystal data		
	Alum-(K)	Voltaite
X-ray formula	$(K_{0.879}Tl_{0.121})(Al_{0.877}Fe_{0.123})(SO_4)_2(H_2O)_{12}$	$(K_{1.872}Tl_{0.128})(Fe_{1.964}Mg_{0.036})(Fe_{2.238}Mg_{0.762})Al(SO_4)_{12}(H_2O)_{18}$
Crystal size (mm)	0.15 × 0.12 × 0.10	0.08 × 0.08 × 0.07
Cell setting, space group	$Pa\bar{3}$	$Fd\bar{3}c$
a (Å)	12.2030(2)	27.2635(18)
V (Å^3)	1817.19(9)	20265(4)
Z	4	16
Data collection and refinement		
Radiation, wavelength (Å)	Mo*K*α, λ = 0.71073	Mo*K*α, λ = 0.71073
Temperature (K)	293	293
Maximum observed 2θ (°)	54.95	54.93
Measured reflections	10598	19025
Unique reflections	705	976
Reflections $F_o > 4\sigma(F_o)$	648	817
R_{int} after absorption correction	0.0284	0.0626
$R\sigma$	0.0110	0.0199
Range of *h*, *k*, *l*	-15 ≤ *h* ≤ 14 -15 ≤ *k* ≤ 11 -15 ≤ *l* ≤ 15	-35 ≤ *h* ≤ 34 -35 ≤ *k* ≤ 26 -30 ≤ *l* ≤ 35
R_1 [F_o>4 σ F_o]	0.0351	0.0434
R_1 (all data)	0.0385	0.0548
wR_2 (on F_o^2)	0.0867	0.1263
Goodness of fit	1.192	1.162
Number of least-squares parameters	61	87
Maximum and minum residual peak (*e*/Å^3)	0.29 [at 0.85 Å from O(4)A] -0.31 [at 0.08 Å from O(3)A]	1.26 [at 1.19 Å from Ow(6)] -0.39 [at 0.61 Å from H(53)]

724

725

726

727

728
729
730

This is a preprint, the final version is subject to change, of the American Mineralogist (MSA)
Cite as Authors (Year) Title. American Mineralogist, in press.
DOI: https://doi.org/10.2138/am-2020-7320

Table 3 – Site occupancy factors (s.o.f.), fractional atom coordinates, and isotropic (*) or equivalent isotropic displacement parameters (in Å^2) for alum-(K) and voltaite. U_{eq} is defined as one third of the trace of the orthogonalized U^{ij} tensor.

Alum-(K)

Site	Wyckoff position	s.o.f.	*x*/*a*	*y*/*b*	*z*/*c*	$U_{eq/iso}$
K	4*b*	$K_{0.879(2)}Tl_{0.121(2)}$	½	½	½	0.0526(4)
Al	4*a*	$Al_{0.877(8)}Fe_{0.123(8)}$	0	0	0	0.0178(4)
S	8*c*	$S_{1.00}$	0.30852(4)	0.30852(4)	0.30852(4)	0.0225(3)
Ow(1)	24*d*	$O_{1.00}$	0.15320(12)	0.01817(13)	-0.01744(13)	0.0256(4)
Ow(2)	24*d*	$O_{1.00}$	0.04621(16)	0.13636(15)	0.30100(15)	0.0374(5)
O(3)	8*c*	$O_{0.770(3)}$	0.2403(2)	0.2403(2)	0.2403(2)	0.0658(15)
O(3)A	8*c*	$O_{0.230(3)}$	0.3761(7)	0.3761(7)	0.3761(7)	0.0658(15)
O(4)	24*d*	$O_{0.770(3)}$	0.2652(2)	0.4209(2)	0.3115(2)	0.0461(8)
O(4)A	24*d*	$O_{0.230(3)}$	0.2873(8)	0.2041(7)	0.3646(8)	0.0461(8)
H(11)	24*d*	$H_{1.00}$	0.205(2)	0.028(3)	0.041(2)	0.066(11)*
H(12)	24*d*	$H_{1.00}$	0.187(2)	0.044(3)	-0.083(2)	0.068(11)*
H(21)	24*d*	$H_{1.00}$	-0.002(3)	0.195(2)	0.291(3)	0.069(11)*
H(22)	24*d*	$H_{1.00}$	0.115(2)	0.168(4)	0.300(4)	0.100(16)*

Voltaite

Site	Wyckoff position	s.o.f.	*x*/*a*	*y*/*b*	*z*/*c*	$U_{eq/iso}$
K	32*b*	$K_{0.936(3)}Tl_{0.064(3)}$	¼	¼	¼	0.0358(9)
M(1)	32*c*	$Fe_{0.982(14)}Mg_{0.018(14)}$	0	0	0	0.0152(5)
M(2)	96*g*	$Fe_{0.746(10)}Mg_{0.254(10)}$	¼	0.10274(3)	-0.10274(3)	0.0170(4)
Al	16*a*	$Al_{1.00}$	1/8	1/8	1/8	0.0129(9)
S	192*h*	$S_{1.00}$	0.23742(4)	0.27552(4)	0.11854(4)	0.0148(3)
O(1)	192*h*	$O_{1.00}$	0.24984(13)	0.24646(13)	0.07377(12)	0.0230(7)
O(2)	192*h*	$O_{1.00}$	0.22466(15)	0.32600(13)	0.10409(14)	0.0298(9)
O(3)	192*h*	$O_{1.00}$	0.19484(15)	0.25393(15)	0.14332(16)	0.0391(10)
O(4)	192*h*	$O_{1.00}$	0.28004(14)	0.27514(15)	0.15208(13)	0.0303(9)
Ow(5)	192*h*	$O_{1.00}$	0.18263(11)	0.41982(12)	0.12142(11)	0.0163(7)
Ow(6)	192*h*	$O_{0.25}$	0.0896(5)	0.1464(6)	0.0703(5)	0.030(2)
Ow(7)	192*h*	$O_{0.25}$	0.0692(5)	0.0889(6)	0.1041(5)	0.030(2)
H(52)	192*h*	$H_{1.00}$	0.172(6)	0.424(3)	0.1530(14)	0.08(2)*
H(53)	192*h*	$H_{1.00}$	0.167(3)	0.433(3)	0.094(2)	0.08(2)*

This is a preprint, the final version is subject to change, of the American Mineralogist (MSA)
Cite as Authors (Year) Title. American Mineralogist, in press.
DOI: https://doi.org/10.2138/am-2020-7320

748 **Table 4** – Selected bond distances (in Å) for alum-(K) and voltaite.

Alum-(K)					
K	– O(3)A (× 2)	2.618(16)	S	– O(3)A	1.429(16)
	– Ow(2) (× 6)	2.9974(19)		– O(3)	1.442(5)
				– O(4)A (× 3)	1.469(8)
Al	– Ow(1) (× 6)	1.8946(14)		– O(4) (× 3)	1.470(2)

Voltaite					
K	– O(4) (× 6)	2.875(4)	Al	– Ow(6)(× 6)	1.868(14)
	– O(3) (× 6)	3.276(5)		– Ow(7) (× 6)	1.900(13)
M(1)	– O1 (× 6)	2.014(3)	S	– O(3)	1.466(4)
				– O(2)	1.473(4)
M(2)	– Ow/5) (× 2)	2.003(3)		– O(4)	1.479(4)
	– O(2) (× 2)	2.062(4)		– O(1)	1.494(4)
	– O(4) (× 2)	2.101(4)			

749

750

This is a preprint, the final version is subject to change, of the American Mineralogist (MSA)
Cite as Authors (Year) Title. American Mineralogist, in press.
DOI: https://doi.org/10.2138/am-2020-7320

751 **Table 5** – Weighted bond valences for alum-(K) and voltaite, in valence units (v.u.).

Alum-(K)

Site	Ow(1)	Ow(2)	O(3)	O(3)A	O(4)	O(4)A	Σ cations
K		$^{6x\rightarrow}$0.09		0.06			0.60
Al	$^{6x\rightarrow}$0.54						3.24
S			1.26	0.39	$^{3x\rightarrow}$1.17	$^{3x\rightarrow}$0.35	6.21
Σ anions	0.54	0.10	1.64[a]	1.75[a]	1.52[a]	1.52[a]	
H–bonds	-0.27 -0.28[b], -0.17[c]	+0.27 -0.17[d] -0.19[e]	+0.19 +0.19 +0.19	-	+0.28 +0.20	+0.17 +0.16 +0.10	
Σ anions$_{corr}$	-0.01[b], 0.10[c]	0.01	2.21[a]	1.75[a]	2.00[a]	1.95[a]	

[a]Assuming the full occupancy of the corresponding O site.
[b]O(4) acceptor
[c]O(4)A acceptor
[d]weighted between O(3) (0.19, s.o.f. 0.77) and O(4)A (0.11, s.o.f. 0.23)
[e]weighted between O(4) (0.20, s.o.f. 0.77) and O(4)A (0.16, s.o.f. 0.23)

Voltaite

Site	O(1)	O(2)	O(3)	O(4)	Ow(5)	Ow(6)/Ow(7)	Σ cations
K			$^{6x\rightarrow}$0.04	$^{6x\rightarrow}$0.13			1.02
M(1)	$^{6x\rightarrow}$0.50						3.00
M(2)		$^{2x\rightarrow}$0.41		$^{2x\rightarrow}$0.37	$^{2x\rightarrow}$0.48		2.52
Al						$^{3x\rightarrow}$0.56 $^{3x\rightarrow}$0.51	3.21
S	1.42	1.50	1.53	1.48			5.93
Σ anions	1.92	1.91	1.57	1.98	0.48	0.56 0.51	
H–bonds	-	+0.13	+0.14 +0.40/+0.30/ +0.20/+0.18[f]	-	-0.13 -0.14	-	-
Σ anions$_{corr}$	1.92	2.04	2.11/2.01/ 1.91/1.89	1.98	0.21	-0.14/+0.13	

[f]values calculated assuming the full-occupancy at Ow(6) and Ow(7)

752

753

This is a preprint, the final version is subject to change, of the American Mineralogist (MSA)
Cite as Authors (Year) Title. American Mineralogist, in press.
DOI: https://doi.org/10.2138/am-2020-7320

754 **Table 6** – EXAFS multiparameter fit details for alum-(K) and voltaite, Tl L_3-edge

	S_0^2	ΔE_0 (eV)	Path	N	R(Å)	σ^2 (Å^2)	*k* range(Å^{-1})	*R-factor*
alum-K	1.1(2)	-7(1)	Tl-O	2	2.66(2)	0.034(5)	2.0-6.3	0.015
			Tl-O	6	2.84(2)	//	//	
			Tl-O	6	3.79(3)	//	//	
voltaite	0.8(3)	3(1)	Tl-O	6	2.89(2)	0.016(6)	2.0-6.1	0.039
			Tl-S	6	3.61(3)	0.018(5)	//	

Notes: S_0^2 = amplitude reduction factor, ΔE_0= shift of the energy origin, R = path length, N = path degeneracy, σ^2 = Debye-Waller factor. Errors, as calculated by ARTEMIS, are indicated in parentheses. *R-factor* is defined as $R = \Sigma(|data - fit|^2) / \Sigma(|data|^2)$.

755

756

757 **Table 7** – Bond lengths (Å), angles (°), and bond strengths (v.u.) for H-bonds in alum-(K) and
758 voltaite.

Alum-(K)						
Donor (*D*)	*D*–H	Acceptor (*A*)	H···*A*	*D*–H···*A* angle	*D*···*A*	bond strength*
Ow(1)–H(11)	0.963(19)	Ow(2)	1.663(19)	176(4)	2.625(2)	0.27
Ow(1)–H(12)	0.950(18)	O(4)	1.663(10)	170(3)	2.604(3)	0.28
Ow(1)–H(12)	0.950(18)	O(4)A	1.95(2)	157(3)	2.848(10)	0.17
Ow(2)–H(21)	0.929(19)	O(4)	1.84(2)	165(4)	2.749(3)	0.20
Ow(2)–H(21)	0.929(19)	O(4)A	1.99(2)	161(3)	2.882(8)	0.16
Ow(2)–H(22)	0.92(2)	O(3)	1.91(3)	158(4)	2.787(3)	0.19
Ow(2)–H(22)	0.92(2)	O(4)A	2.29(3)	155(4)	3.153(11)	0.11
Voltaite						
Donor (*D*)	*D*–H	Acceptor (*A*)	H···*A*	*D*–H···*A* angle	*D*···*A*	bond strength*
Ow(5) – H(52)	0.92(2)	O(2)	2.07(2)	173(15)	2.990(5)	0.13
Ow(5) – H(53)	0.92(2)	O(3)	2.13(5)	148(7)	2.955(5)	0.14

759 *Calculated according to Ferraris and Ivaldi (1988).
760
761

This is a preprint, the final version is subject to change, of the American Mineralogist (MSA)
Cite as Authors (Year) Title. American Mineralogist, in press.
DOI: https://doi.org/10.2138/am-2020-7320

762 **Fig. 1** – Tl-bearing sulfates from the Fornovolasco mining complex. (a) Alum-(K) as colorless
763 crystalline masses associated with römerite, copiapite, and minor voltaite. (b) Voltaite, {100}
764 individuals with minor {111} and {110} faces, associated with a tabular crystal of alunogen.

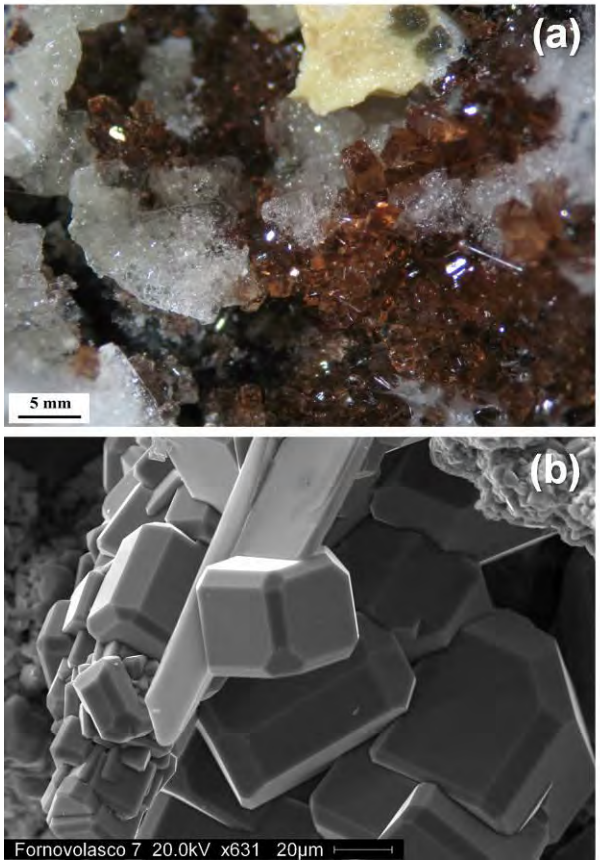

765

766

This is a preprint, the final version is subject to change, of the American Mineralogist (MSA)
Cite as Authors (Year) Title. American Mineralogist, in press.
DOI: https://doi.org/10.2138/am-2020-7320

767 **Fig. 2** – Crystal structure of alum-(K), as seen down **a**, and the two different SO_4 configurations,
768 not bonded (b) and bonded to K^+ (c). Dark grey and grey polyhedra represent Al and S sites,
769 respectively. Dark grey, grey, and light grey small circles represent O, H, and Ow sites,
770 respectively, whereas the K site is shown as large dark grey circles.

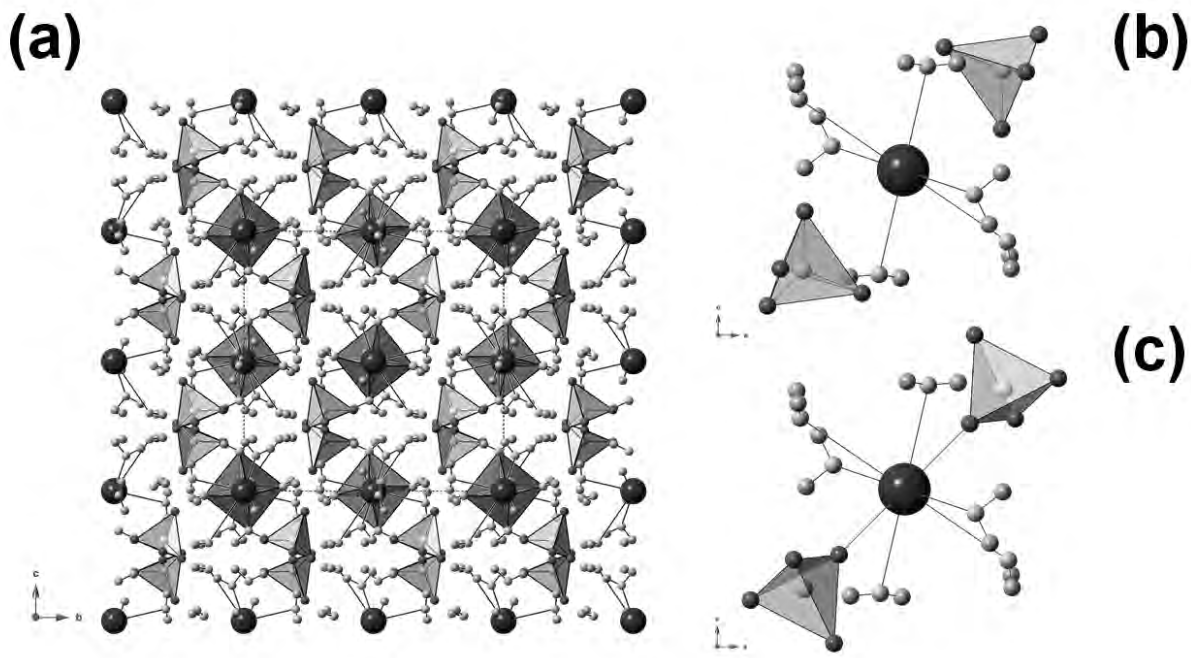

771

772

This is a preprint, the final version is subject to change, of the American Mineralogist (MSA)
Cite as Authors (Year) Title. American Mineralogist, in press.
DOI: https://doi.org/10.2138/am-2020-7320

773 **Fig. 3** – Micro-Raman (a) and FTIR (b) spectra of alum-(K) and band interpretation. The
774 deconvolution of the O–H stretching region and the ν_1 (SO_4) modes in the Raman spectrum are
775 shown on upper left and right in (a), respectively.

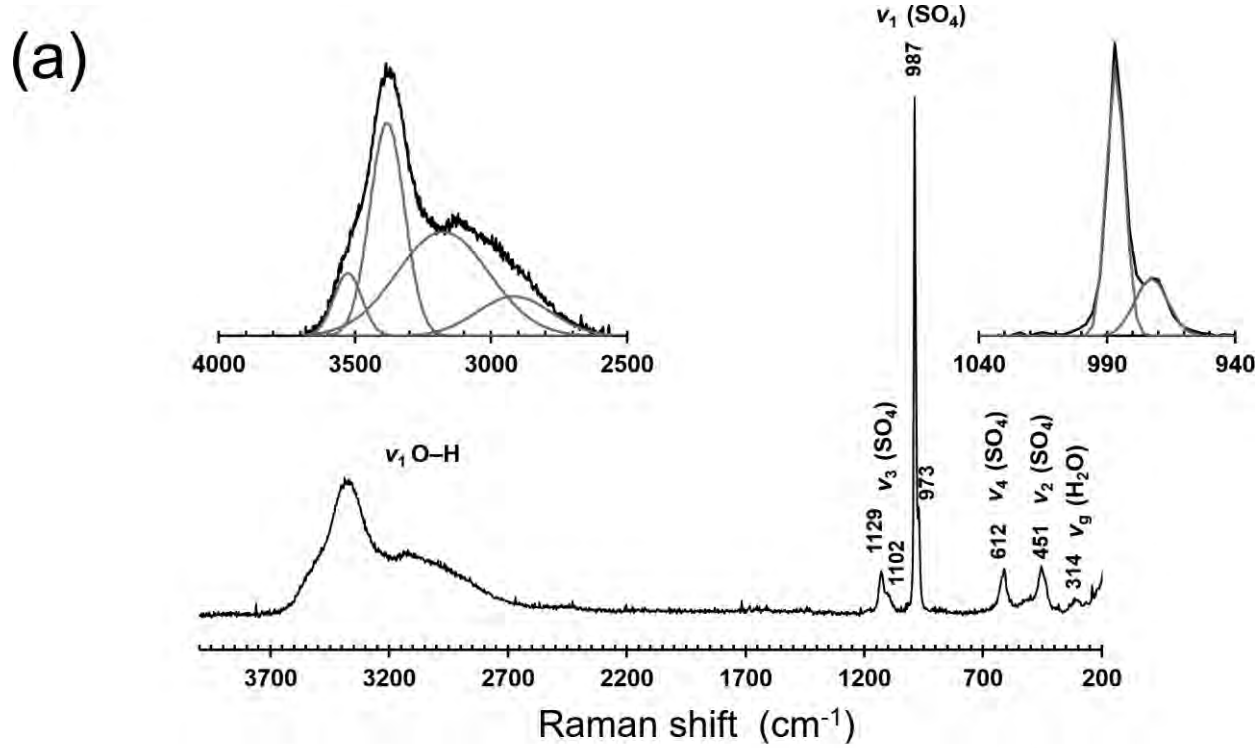

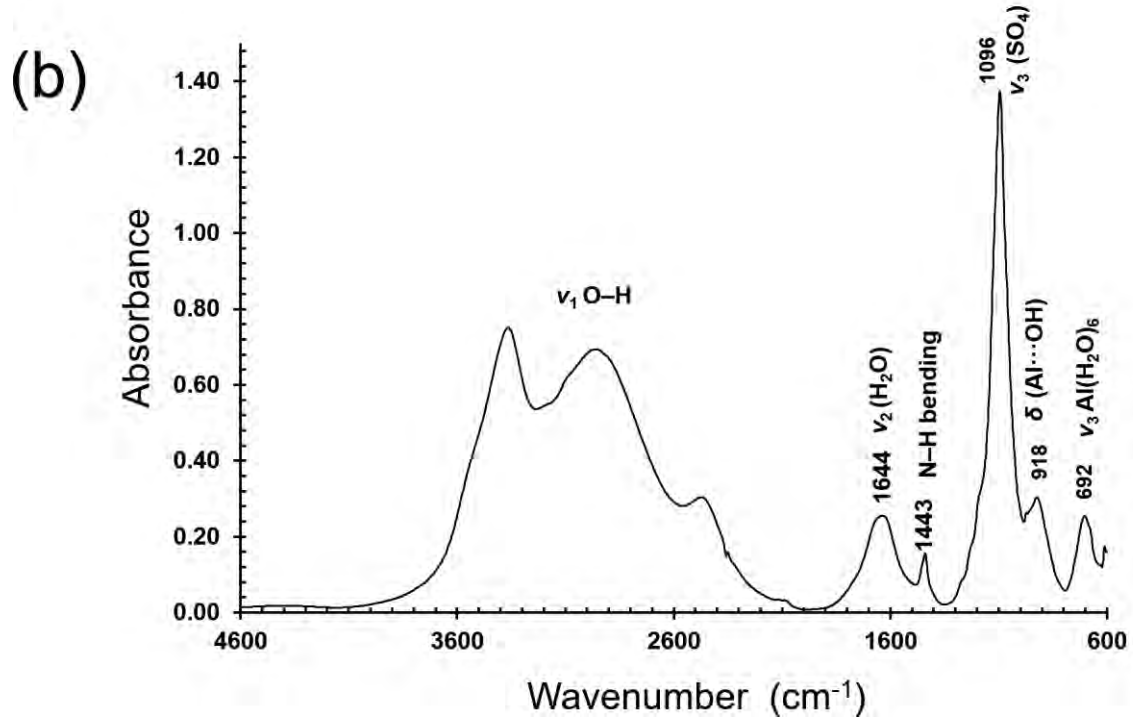

776

777

This is a preprint, the final version is subject to change, of the American Mineralogist (MSA)
Cite as Authors (Year) Title. American Mineralogist, in press.
DOI: https://doi.org/10.2138/am-2020-7320

778 **Fig. 4** – a) Normalized Tl-L_3 edge XANES for alum-(K), voltaite and model compounds. Tl L_3 edge
779 EXAFS (a) and Fourier transform (b) of voltaite and alum-K. Black lines are data, open squares are
780 fits.

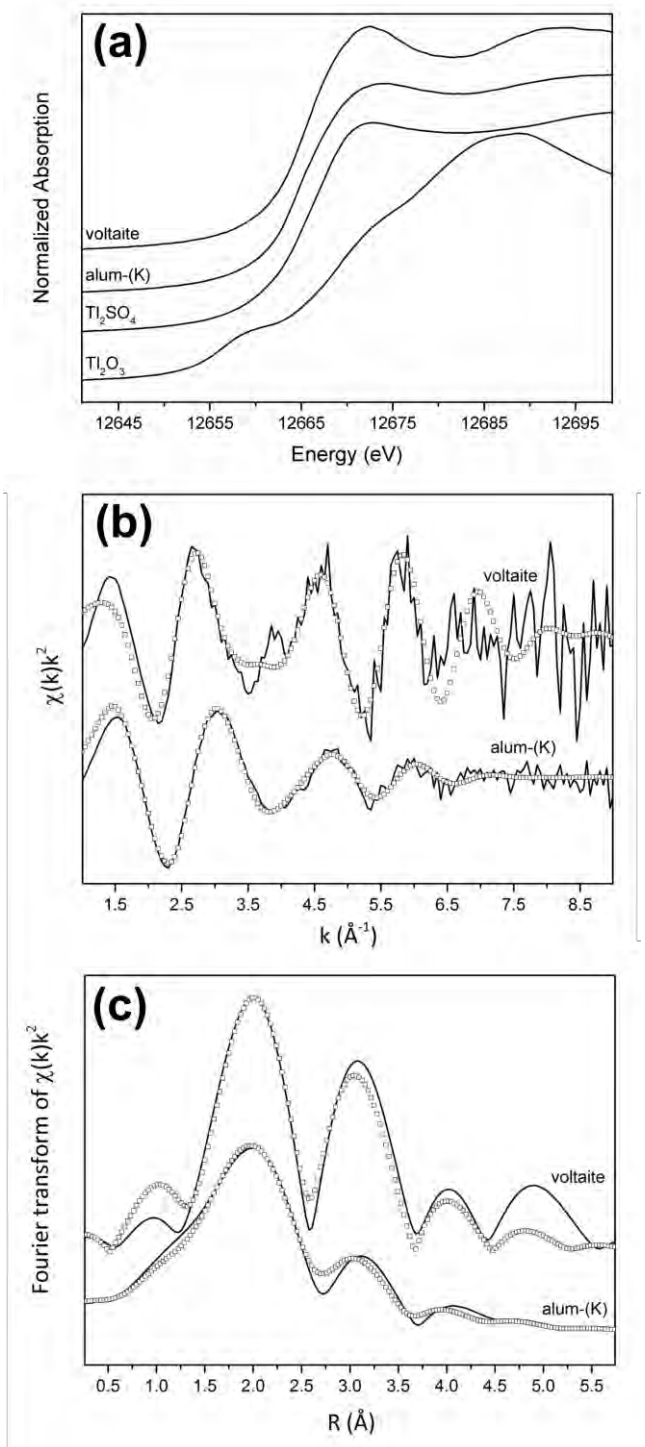

781

782

This is a preprint, the final version is subject to change, of the American Mineralogist (MSA)
Cite as Authors (Year) Title. American Mineralogist, in press.
DOI: https://doi.org/10.2138/am-2020-7320

783 **Fig. 5** – Crystal structure of voltaite, as seen down **a** (a). Polyhedra: dark grey = *M*(1) site; grey =
784 *M*(2) site; light grey = S site. Small circles: dark grey = Al site; light grey = O atoms bonded to H
785 atoms, forming H_2O groups;; grey = O atoms. Large dark grey circles = K site. The disordered H_2O
786 groups around Al atoms are shown. Hydrogen atoms are not shown. In (b), an ordered Al-centered
787 octahedron is shown down [111], along with the H-bond system. Same symbols as in (a), with the
788 exception of Ow(6) and Ow(7) sites, shown as grey and black circles, respectively. Dashed lines
789 represent H-bonds.

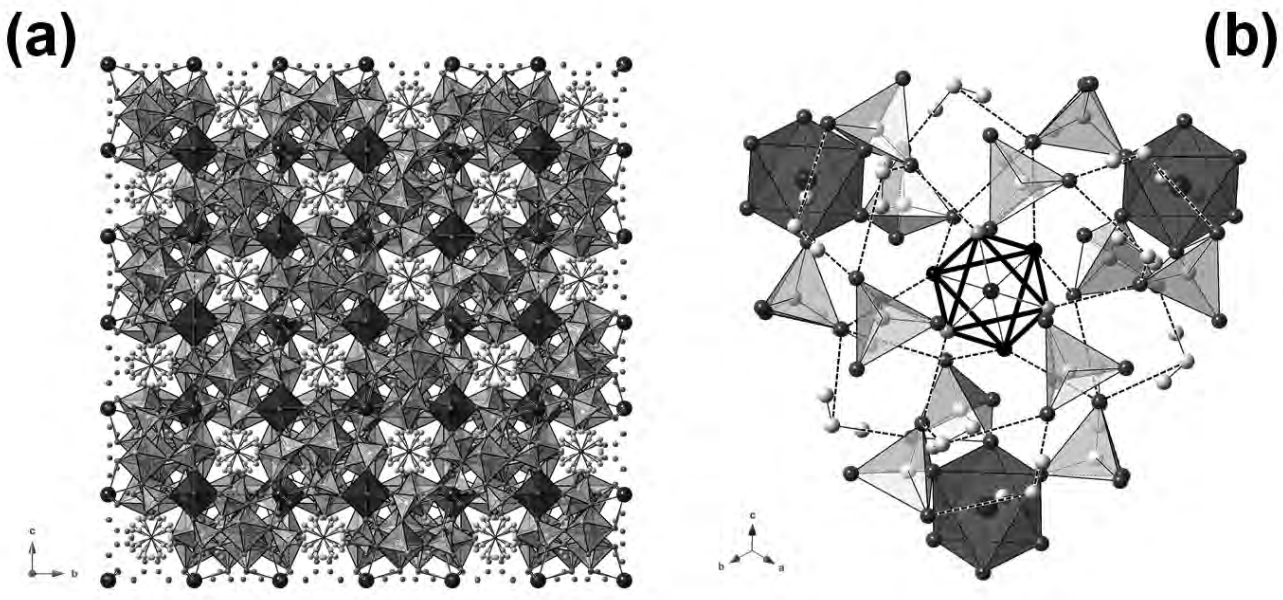

790
791

792 **Fig. 6** – Mössbauer spectrum of voltaite obtained at room-temperature. Fitted absorption doublets
793 assigned to Fe^{2+} and Fe^{3+} are indicated by dashed and dotted lines, respectively. Diamonds denote
794 measured spectrum and black curve represents summed fitted doublets.

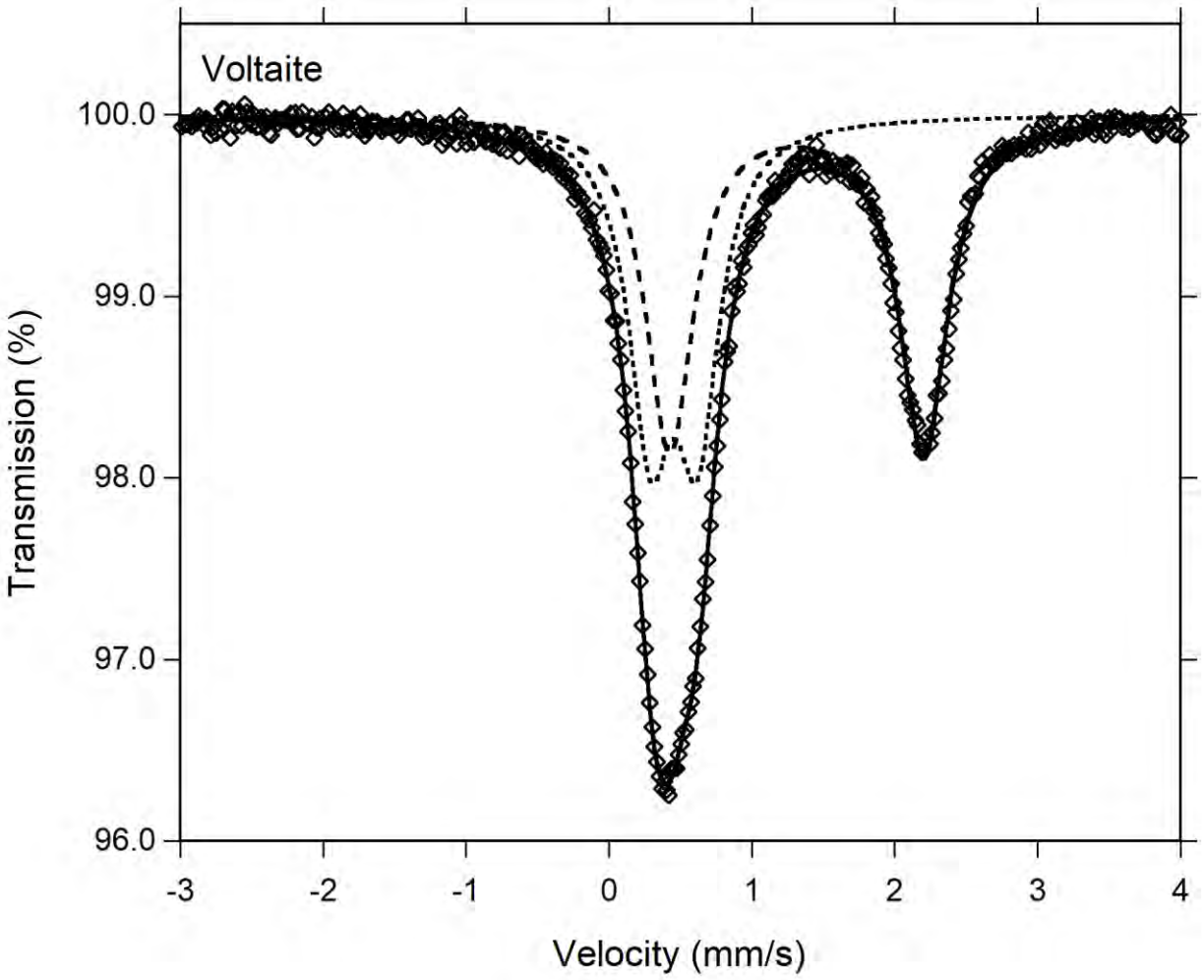

795
796
797

This is a preprint, the final version is subject to change, of the American Mineralogist (MSA)
Cite as Authors (Year) Title. American Mineralogist, in press.
DOI: https://doi.org/10.2138/am-2020-7320

798 **Fig. 7** – FTIR (a) and Raman (b) spectra of voltaite and band interpretation.

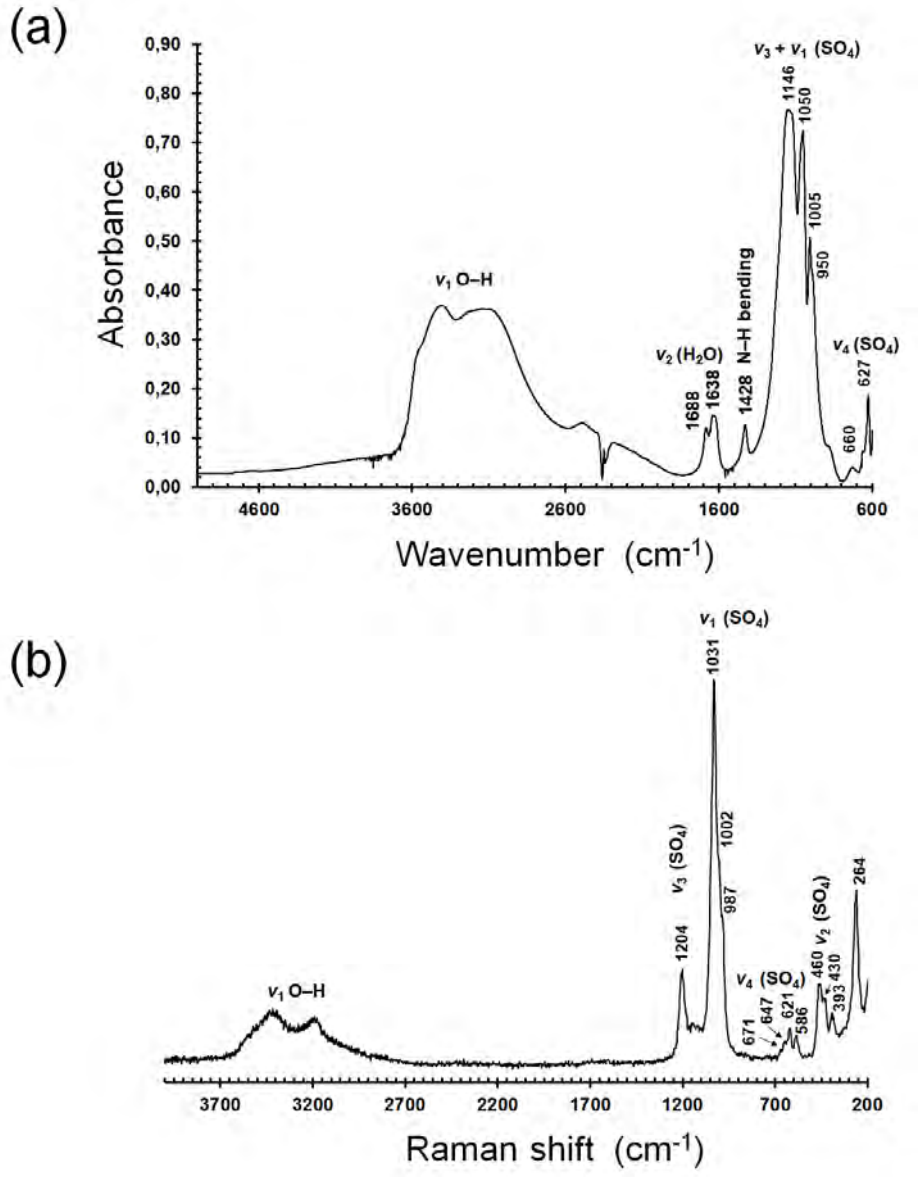

799

800

801